

q -deformed evolutionary dynamics in simple matrix games

Christopher R. Kitching^{1,*} and Tobias Galla^{2,†}

¹*Department of Physics and Astronomy, School of Natural Sciences,*

The University of Manchester, Manchester M13 9PL, UK

²*Instituto de Física Interdisciplinar y Sistemas Complejos, IFISC (CSIC-UIB),*

Campus Universitat Illes Balears, E-07122 Palma de Mallorca, Spain

(Dated: July 24, 2024)

We consider evolutionary games in which the agent selected for update compares their payoff to q neighbours, rather than a single neighbour as in standard evolutionary game theory. Through studying fixed point stability and fixation times for 2×2 games with all-to-all interactions, we find that the flow changes significantly as a function of q . Further, we investigate the effects of changing the underlying topology from an all-to-all interacting system to an uncorrelated graph via the pair approximation. We also develop the framework for studying games with more than two strategies, such as the rock-paper-scissors game where we show that changing q leads to the emergence of new types of flow.

I. Introduction

Modern game theory was pioneered by mathematician John von Neumann in the 1920s to mathematically model strategic interactions among agents whose decisions are rational [1–3]. In the 1970s John Maynard Smith and George Price built on this idea by introducing evolutionary game theory [4, 5]. Here, agents do not act rationally, instead each individual carries a particular strategy that is passed on from parent to offspring. Reproduction occurs in proportion to fitness. This was initially conceived as a model of Darwinian evolution in biology, but has also found applications in the social sciences and in economics [6]. Originally, evolutionary game dynamics in populations were described mostly by deterministic differential equations, such as the commonly used replicator equations [7]. These equations are formally valid for infinite populations.

However, it is now well established that stochastic effects can considerably affect the outcome of evolution (see e.g. [8–10]). There is thus a continuously growing body of work on evolutionary game theory in finite populations. One particular focus is also on networked populations, that is, population in which any one individual can only interact and compete with its immediate neighbours. This has sometimes been referred to as ‘evolutionary graph theory’ [11]. This should not be misunderstood as a theory of evolving graphs. Despite the terminology, the underlying graph does often not change in time.

The starting point for studies of evolutionary game theory in finite populations and networks is usually an individual-based model. This is a set of rules by which the agents interact and the population evolves. A number of different interaction models have been

proposed, see e.g. [12, 13]; a summary can also be found in [14]. For analytical convenience the total size of the population is often kept fixed. Here, we focus on the so-called pairwise comparison process mediated via ‘Fermi functions’ [15]. Detailed definitions will be given in Sec. II.

The so-called voter model is a related, but different model of interacting individuals. It was originally introduced by Holley and Liggett in 1975 to model interacting particle systems [16]. In the most basic voter model, the population consists of voters which are of binary types (‘opinions’), 0 or 1, connected in some way through a network. In each step of the dynamics one randomly chosen individual adopts the opinion of a randomly chosen neighbour. Many extensions and variations of this model have been proposed and studied [17–21]. One such variation is the so-called ‘ q -voter model’, in which q neighbours need to agree with one another in order for a voter to change opinion [22–24].

In this paper we seek to combine the ideas of evolutionary games and the q -voter model into ‘ q -deformed’ evolutionary game dynamics. We consider a population of individuals who each carry a particular strategy, and the population then evolves following rules similar to those in conventional models of evolutionary game theory, in particular the probability for an agent to change state depends on payoff. However, before a change can occur, an agent must consult with q of its neighbours. As in the q -voter model a change of that agent can then only occur if all those q neighbours are of the same type. As we will show this can significantly affect the evolutionary flow in strategy space, and quantities such as fixation probabilities and times in finite populations.

The remainder of the paper is organised as follows. In Sec. II we introduce the model of q -deformed evolutionary game dynamics for 2×2 games (two-strategy two-player games). In Sec. III we investigate the rate equations for the q -deformed dynamics in infinite all-to-all populations. We study the fixed points and

* christopher.kitching@manchester.ac.uk

† tobias.galla@ifisc.uib-csic.es

their stability, and show that the type of evolutionary flow changes as a function of q . In Sec. IV we look at fixation times and probabilities in finite all-to-all systems. In Sec. V we study the effects of changing the underlying topology from a complete graph to an uncorrelated graph. Analytical results for q -deformed dynamics are obtained within the pair approximation. In Sec. VI we study games with more than two strategies. We investigate cyclic games (motivated by the familiar rock-paper-scissors game) as an example and show that q -deformation can induce new behaviour, in particular the emergence of stable limit cycles. Finally in Sec. VII we look at a modified version of the model, where we select the q -neighbours without replacement. We summarise our results in Sec. VIII, and give an outlook on possible future work.

II. Model definitions

A. Payoff matrix

We consider a population of N agents, who are each of type A or B . For the time being we always consider a population with all-to-all interaction.

The game is defined by the 2×2 payoff matrix

$$\begin{matrix} & \begin{matrix} A & B \end{matrix} \\ \begin{matrix} A & B \end{matrix} & \begin{pmatrix} a & b \\ c & d \end{pmatrix} \end{matrix}. \quad (1)$$

An A agent interacting with another A agent thus receives payoff a , and it receives b if interacting with an agent of type B . Likewise a B agent receives c when interacting with an A , and d when interacting with a B .

In finite systems we characterise the state by the number of type A agents i , or, equivalently, by the fraction of A agents in the population, $x = i/N$. The expected payoff for type A and B agents respectively is then

$$\begin{aligned} \pi_A(x) &= ax + b(1-x), \\ \pi_B(x) &= cx + d(1-x). \end{aligned} \quad (2)$$

We can define the payoff difference as

$$\Delta\pi(x) = \pi_A(x) - \pi_B(x) = ux + v, \quad (3)$$

where,

$$\begin{aligned} u &= (a + d) - (b + c), \\ v &= b - d. \end{aligned} \quad (4)$$

For evolutionary processes relying only on payoff differences it is thus possible to represent the payoff matrix in Eq. (1) with only two variables: u and v .

B. q -deformed evolutionary dynamics

At each time step we randomly choose an agent for update, say it is of type A . We then choose q agents from the population (with replacement). If all those agents are of type B , then the A switches to B , with a probability g^- that depends on the payoffs of type A and B agents. Similarly, we write g^+ for the probability for a B to switch to A if q other randomly selected agents also are of type A .

There are many possible choices for the functions g^\pm . One such choice is to make g^\pm proportional to the payoff of the type that is being switched to, i.e.

$$g^\pm(x) = \frac{\pi_{A/B}(x)}{\max\{a, b, c, d\}}. \quad (5)$$

This choice is only valid if all entries in the payoff matrix are positive. The denominator ensures that $g^\pm(x) \leq 1$. In this way, if type B agents have a large average payoff, then type A agents are likely to switch during interactions with them. But it is still possible for an agent to switch to a type with a lower expected payoff than its current type. A second popular choice involves non-linear Fermi functions g^\pm [15, 25],

$$g^\pm(x) = \frac{1}{1 + e^{\mp\beta\Delta\pi(x)}}. \quad (6)$$

These depend on the payoff difference. The parameter $\beta \geq 0$, known as the intensity of selection, reflects the uncertainty in decision-making processes. In the strong selection limit, $\beta \rightarrow \infty$ an individual will always switch to the type with the higher expected payoff. For any finite β the reverse process occurs with non-zero probability. For $\beta = 0$ one has $g^\pm = \frac{1}{2}$, i.e. neutral selection. Payoffs then have no effect. Since the parameter β only appears in combination with u and v , we will absorb it into those parameters, effectively setting $\beta = 1$.

The rates at which the type A and B agents switch are given by,

$$\begin{aligned} T^+(x) &\equiv T_{B \rightarrow A}(x) = N(1-x)x^q g^+(x), \\ T^-(x) &\equiv T_{A \rightarrow B}(x) = Nx(1-x)^q g^-(x), \end{aligned} \quad (7)$$

respectively. The first expression can be understood as follows. The agent chosen for reproduction is of type B with probability $1-x$. The probability that q randomly chosen neighbours (with replacement) in this all-to-all population are all of type A is x^q . The type B agent switches to type A with probability $g^+(x)$. We will sometimes write T_i^\pm instead of $T^\pm(x)$, noting that $x = i/N$.

We measure time in units of generations, the rates are therefore proportional to the size N of the population. While the above motivation of the model implicitly assumes that q is a positive integer, the continuous-time rates in Eq. (7) are mathematically

meaningful for all $q > 0$. We thus treat $q > 0$ as a real-valued model parameter, similar to what is done in the literature on the q -voter model [23, 24, 26–29]. For $q = 1$ the setup reduces to that of conventional evolutionary game theory in finite populations (see e.g. [9, 10, 14, 30]). We will refer to choices $q \neq 1$ as a ‘ q -deformation’ of the dynamics.

It is easy to understand that q -deformation favours strategies that are in the minority when $q < 1$, or in majority respectively, for $q > 1$. To see this it is useful to focus on the case with no selection ($g^\pm \equiv 1/2$ in our notation). If the frequency of strategy A is x , the rate of change from A to B is proportional to $x(1-x)^q$ and that for the reverse change proportional to $x^q(1-x)$. For $q = 1$ these terms balance for all x . This is the case of the conventional voter model, where there is no deterministic drift. For $q < 1$ we have $x(1-x)^q < (1-x)x^q$ when $x < 1/2$. Thus for $q < 1$ strategy A is favoured when it is in the minority, and disfavoured when more than half of population is of type A . The direction of the flow reverses for $q > 1$.

III. Rate equations for infinite populations

A. q -deformed rate equations

For large populations the average dynamics of the population is approximated by a q -deformed version of the conventional rate equations in an infinite population. This is explained further in the Supplemental Material (SM) [31], see in particular Sec. S1. We have

$$\dot{x} = (1-x)x^q g^+(x) - x(1-x)^q g^-(x). \quad (8)$$

The quantity x in this equation is really $\langle x \rangle$, an average over individual realisations of the dynamics. However to ease notation we will write x throughout. Also note if we choose g^\pm as in Eq. (5), then after absorbing the constant by re-scaling time we find,

$$\dot{x} = (1-x)x^q \pi_A(x) - x(1-x)^q \pi_B(x). \quad (9)$$

This is a q -deformed variant of the conventional replicator equations. Setting $q = 1$ reduces this to the standard replicator equation for 2-player 2-strategy games [32],

$$\dot{x} = x(1-x) [\pi_A(x) - \pi_B(x)]. \quad (10)$$

Given an initial distribution of type A and B agents in a population, Eq. (8) determines how the composition of the population changes with time. The system will eventually reach a fixed point. The location of the fixed point depends on u and v , and (potentially) on the initial condition. Our first step is therefore an analysis of the fixed points of the q -deformed rate equations and of the stability of these fixed points. As a benchmark we first summarise the well-known results for the case $q = 1$.

B. The case $q = 1$

The simplest case is that of $q = 1$, where Eq. (8) reduces to

$$\dot{x} = x(1-x)[g^+(x) - g^-(x)]. \quad (11)$$

In this case, there are always two fixed points at the boundaries, $x^* = 0, 1$. There is also potentially a third, interior, fixed point given by the solution of $g^+(x^*) = g^-(x^*)$. For the functions in Eqs. (5) and (6), this equates to solving $\Delta\pi(x^*) = 0$, so

$$x^* = \frac{-v}{u} = \frac{b-d}{c-a+b-d}. \quad (12)$$

For some values of u and v this solution is unphysical ($x^* < 0$ or $x^* > 1$). We then only have the fixed points at $x^* = 0$ and $x^* = 1$. In the special case $a = c$ and $b = d$ (neutral selection) we have $\dot{x} = 0$, in which case every point x is a fixed point.

Given values for u and v we can characterise the type of flow based on the number of fixed points and their linear stability. From Eq. (11), if $g^+(0) > g^-(0)$ then $x^* = 0$ is unstable. If $g^+(1) > g^-(1)$ then $x^* = 1$ is a stable fixed point. If an interior fixed point x^* exists, it is stable if

$$\frac{d}{dx} [g^+(x) - g^-(x)] \Big|_{x^*} < 0. \quad (13)$$

These scenarios are summarised in Fig. 1. They are conventionally referred to as the dominance of A or B , ‘co-existence’ or ‘co-ordination’, respectively [10].

We can create a phase diagram in the (u,v) -space to demonstrate how the evolutionary flow changes when we alter the payoff matrix. Fig. 2 shows how this space divides into four regions with the four types of flow. The diagram is valid for the choices of g^\pm in Eqs. (5) and (6). In the case of co-existence or co-ordination, the interior fixed point can vary on the interval $(0, 1)$ which is represented by the opacity of those regions. The shape of these regions can be explained as follows. We have one interior fixed point when $0 < x^* < 1$ and from Eq. (12) this implies $0 < \frac{-v}{u} < 1$. When $u > 0$ we find that $v < 0$ and $v > -u$, this defines the red region in Fig. 2. We then evaluate Eq. (13) at $x^* = \frac{-v}{u}$, to find that $u > 0$ means that the interior fixed point is unstable, hence one has co-ordination type flow [Fig. 1]. Similar analyses can be carried out for the other regions. We note here how the co-existence and co-ordination games blend into dominance games as we change u and v , since their interior fixed points move closer to the boundaries, eventually being absorbed.

C. The case $q \neq 1$

We now focus on the case $q \neq 1$ in Eq. (8). Much like the $q = 1$ case we always have fixed points at

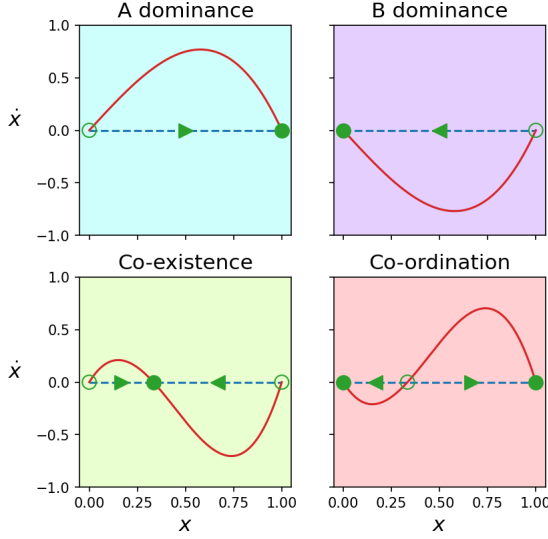


FIG. 1. Classifications of the deterministic dynamics for $q = 1$, Eq. (11). Each classification has an associated colour for easy identification in other plots. Arrows indicate the direction of the flow. Filled/empty green circles are stable/unstable fixed points.

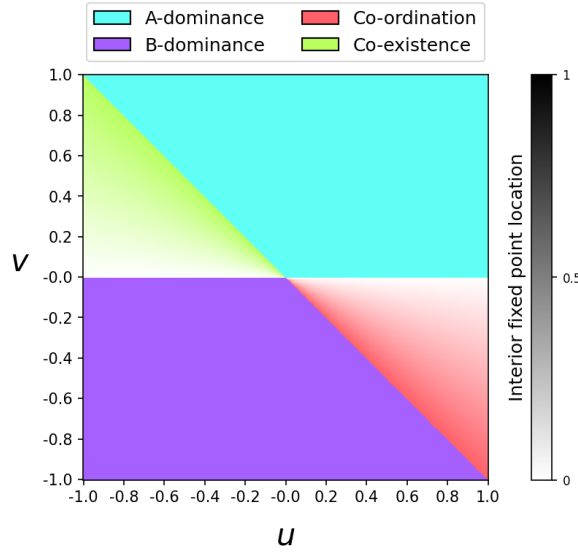


FIG. 2. Phase diagram in (u,v) -space showing the classification regions for evolutionary flow for $q = 1$, Eq. (11). The four colours represent the four possible classifications. The co-existence and co-ordination regions have varying opacity to represent the position of the interior fixed point on the interval $(0, 1)$.

the boundaries, $x^* = 0$ and $x^* = 1$. The number of interior fixed points depends on the functions g^\pm .

All results in this section are for the Fermi function Eq. (6). We find that there can be between one and three interior fixed points. For $q > 1$, we only find co-ordination type flows (i.e. flows with stable fixed

points at the boundaries), and for $q < 1$ we only find co-existence type flows (i.e. flows with unstable fixed points at the boundaries) [see SM, Sec. S2]. This is because the q -deformation favours majority strategies for $q > 1$, while the minority strategy has an advantage for $q < 1$. The possible types of flow of Eq. (8) include standard co-ordination and co-existence as shown in Fig. 1 and the additional types shown in Fig. 3. The left column shows co-existence type behaviour. The right column shows co-ordination type dynamics.

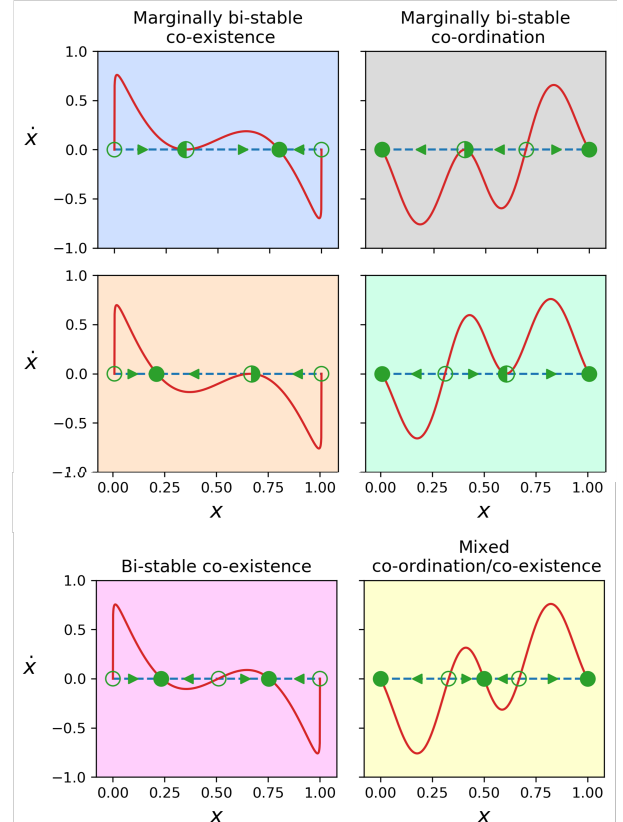


FIG. 3. Possible classifications of the $q \neq 1$ game dynamical flow in Eq. (8), with g^\pm Fermi functions as in Eq. (6). The left column shows $q < 1$ co-existence type games, and the right column shows $q > 1$ co-ordination type games. Each classification has an associated colour for easy identification in other plots.

Even though mathematically we might classify a flow as co-ordination, co-existence or one of the new types, the interior fixed point(s) are often close to $x = 0$ or $x = 1$. The behaviour is then more like a dominance scenario. It is often insightful to plot \dot{x} as a function of x for specific parameters u, v and q .

For the remainder of this section we focus on $q > 1$ (we study the case $q < 1$ in the SM, see for example Fig. S1). Figure 4 is analogous to Fig. 2, except now $q = 2$. What was previously a co-existence region for $q = 1$ is now bi-stable co-ordination. What was A/B -dominance for $q = 1$ is now classified as co-ordination

so there is one large co-ordination region where the position of the interior fixed point varies continuously. The upper and lower boundaries between the mixed co-ordination/co-existence and co-ordination regions are where marginally bi-stable co-ordination occurs.

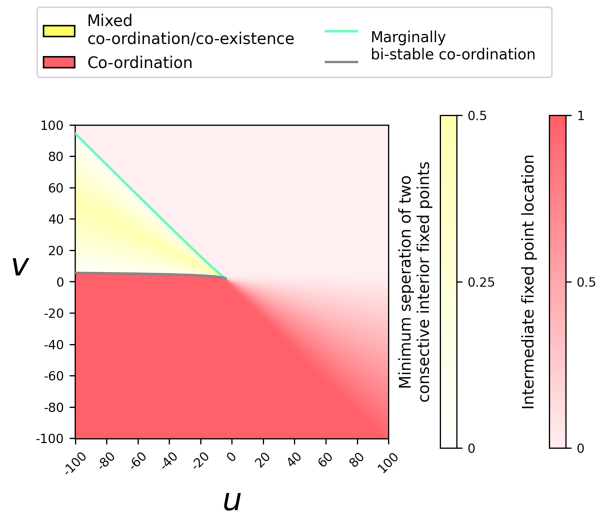


FIG. 4. A phase diagram in (u, v) -space showing the classification regions for the dynamics in Eq. (8) for $q = 2$, and with g^\pm Fermi functions as in Eq. (6). The opacity of the red region represents the position of the single unstable interior fixed point present in co-ordination type flows on the interval $(0, 1)$. The opacity of the yellow region represents the minimum distance between two consecutive interior fixed points in mixed co-ordination/co-existence type flows.

As we increase q , the shapes of these regions change. We can choose particular values of u and v , and investigate how the fixed points move as q is varied. This leads to a bifurcation diagram, as shown in Fig. 5. For $q \leq 1$ and this particular choice of u and v we would have a co-existence type flow, the single interior fixed point is stable. For $q > 1$ we move into a mixed co-ordination/co-existence regime, and two new interior fixed points spawn at the boundaries, both of which are unstable. As q increases further the stable interior fixed point and one of the unstable interior fixed points move closer to one another, and meet at $q \approx 2.15$. Beyond this point, we find one interior fixed point, which is now unstable. This means that the flow is of the co-ordination type. The diagram confirms that small values of q promote the minority strategy, i.e. if only a small fraction of individuals are of type A , then x will increase, and if only a small fraction of individuals are of type B then x will decrease. This produces a stable internal fixed point (co-existence). Conversely, large values of q promote the majority strategy, leading to co-ordination type flows.

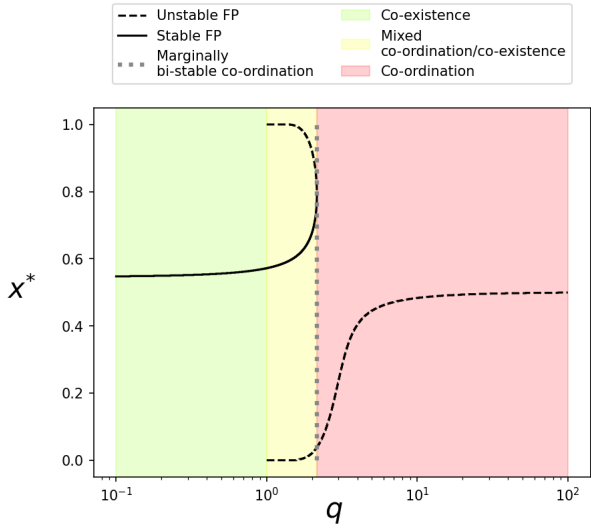


FIG. 5. Bifurcation diagram showing how the interior fixed points change as the value of q changes. Solid lines show stable fixed points, dashed lines indicate unstable fixed points. The figure is for $u = -7$, $v = 4$. Coloured regions classify the type of game (see Fig. 1).

IV. Fixation probability for a single invader, and fixation times

Having analysed the q -deformed deterministic dynamics in infinite populations, we now look at the fixation probabilities and times in finite populations. We will focus on the Fermi update in Eq. (6). Our analysis follows the steps established for example in [30].

The fixation probability ϕ_i is the probability that the evolutionary process ends in a state in which the entire population is of type A (as opposed to entirely of type B), if there are initially i type A individuals (and $N - i$ type B individuals). The conditional average time to fixation t_1^A is the expected time a single invader of type A needs to take over a population consisting initially of $N - 1$ individuals of type B , given such a takeover happens. The unconditional average time to fixation t_1 is the expectation value of the time until the population is monomorphic ($i = 0$ or $i = N$) if there is initially one individual of type A and $N - 1$ individuals of type B .

For the rates in Eq. (7), the probability ϕ_i is given by (see SM, Sec. S3 A)

$$\phi_i = \frac{1 + \sum_{k=1}^{i-1} f_k^{q-1} e^{-H_k}}{1 + \sum_{k=1}^{N-1} f_k^{q-1} e^{-H_k}}. \quad (14)$$

Here, f_k is defined as

$$f_k \equiv f(k; N) = \frac{(-1)^k (1 - N)_k}{k!}, \quad (15)$$

where $(\cdot)_k$ is the Pochhammer symbol [33]. The ob-

ject H_k is defined as

$$H_k \equiv H(k; u, v, N) = k^2 \frac{u}{2N} + k \left(\frac{u}{2N} + v \right). \quad (16)$$

The fixation times can then be written (see SM, Sec. S3B) as

$$t_1 = \phi_1 \sum_{k=1}^{N-1} \sum_{l=1}^k \frac{1}{T_l^+} \left(\frac{f_k}{f_l} \right)^{q-1} e^{-(H_k - H_l)}, \quad (17a)$$

$$t_1^A = \sum_{k=1}^{N-1} \sum_{l=1}^k \frac{\phi_l}{T_l^+} \left(\frac{f_k}{f_l} \right)^{q-1} e^{-(H_k - H_l)}. \quad (17b)$$

In Fig. 5 we showed how the interior fixed points, and hence the type of the evolutionary flow, change with q for a fixed choice of u and v . In Fig. 6 we plot the unconditional and conditional fixation times [Eqs. (17a) and (17b)] as well as the fixation probability [Eq. (14)] as functions of q , for the same game as in Fig. 5, and for a population of size $N = 10$.

For $q < 1$ this particular system is of the co-existence type (green region in Figs. 5 and 6). Thus we expect trajectories of the stochastic dynamics for finite N to move towards the co-existence fixed point, and then to remain near this meta-stable state until a large fluctuation drives the mutant to extinction or fixation. The escape time depends on the population size (the larger the population, the more difficult is the escape) and on the strength of the attraction of the fixed point. In the region $q < 1$ the co-existence fixed points becomes less attractive as q is increased (this is because for small q , the deformation favours the minority strategy). This is in-line with the decrease of fixation times in Fig. 6. Consistent with this, the fixation probability decreases (from approximately 0.98 to 0.94 as q changes from 0.1 to 1). This behaviour is not materially changed by the appearance of two additional unstable fixed points at $q = 0$ (yellow region in Figs. 5 and 6).

For $q \gtrsim 2.15$ the deterministic system is of the co-ordination type (red region in Figs. 5 and 6). We then find that the evolutionary flow becomes smaller in absolute terms as q is increased. This flow is given by the right-hand side of Eq. (8), and describes the net change of the system per unit time. For large q actual events only occur very rarely in time, as changes in the population only happen when a sample of q players all have the same type. Mathematically, the factors x^q and $(1-x)^q$ become small when $x \neq 0, 1$. Thus, the population dynamics becomes slower as q is increased, in-line with the increase of the fixation times in the red region of Fig. 6.

The fixation probability is not affected by time scales, but instead by the ratio of transition rates $T^-(x)/T^+(x)$, as detailed in Eq. (S15) in the SM.

Using Eqs. (6) and (7) we have

$$\frac{T^-(x)}{T^+(x)} = \left(\frac{1-x}{x} \right)^{q-1} e^{-(ux+v)}. \quad (18)$$

For large q , the pre-factor $[(1-x)/x]^{q-1}$ dominates this expression. If x is near zero the pre-factor is large, and thus, with overwhelming probability the next event in the population will lead to a decrease in mutant numbers. Similarly, when x is near one, the pre-factor is small, and the next event in the population is very likely to lead to an increase of the number of mutants. In essence, q -deformation favours the majority type for $q > 1$, and promotes co-ordination. As illustrated in Fig. S2 in the SM this effect becomes stronger as q is increased. Thus, it becomes more difficult for a single mutant to take over the population, and ϕ_1 decreases with q in the co-ordination regime, as seen in the lower panel of Fig. 6.

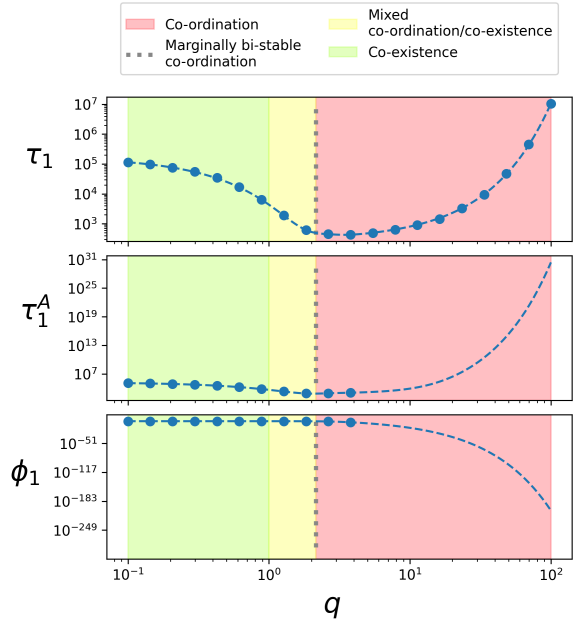


FIG. 6. Conditional fixation time t_1^A (upper panel), unconditional fixation time t_1 (middle panel) and fixation probability ϕ_1 (lower panel) varying with q for $u = -7$, $v = 4$ and $N = 10$ [Fig. 5 shows the corresponding bifurcation diagram for the same game (same u and v)]. Markers are results from averaging over 1×10^3 independent simulations of a population evolving via the process described by Eqs. (6) and (7). Dashed lines are from the theory [Eqs. (14), (17a) and (17b)]. Coloured regions indicate the type of flow (see Fig. 1).

V. q -deformed dynamics on graphs

So far we have only considered populations with all-to-all connectivity, i.e. the dynamics runs on a

complete graph. We now extend the model to more general networks.

The dynamics on graphs are as follows. A random node is selected. In a second step q random neighbours of that node are chosen at random with replacement. If all q neighbours are in the opposite state to that of the node, it will change its state with a specific probability. This probability is as in Eq. (6), but the payoff difference that enters into the functions g^\pm is now

$$\Delta\pi_{n,k} = u\frac{n}{k} + v. \quad (19)$$

Here n is the number of A type neighbours of the node chosen for potential update, and k is its degree. The quantities u and v are as in Eq. (4). Thus, $\Delta\pi_{n,k}$ is the change in the expected payoff of the focal node if it switches from B to A .

Using the pair approximation we can derive differential equations that can be numerically integrated to approximately describe the density of type A agents, x , and the density of ‘active links’, σ , on infinite uncorrelated graphs (see SM, Sec. S4). A link in the network is said to be active when it connects two individuals of different types. These equations are of the form

$$\frac{dx}{dt} = \sum_k P_k \sum_{n=0}^k \left[(1-x) \left(\frac{n}{k} \right)^q g_{n,k}^+ B_-(n|k) - x \left(\frac{k-n}{k} \right)^q g_{n,k}^- B_+(n|k) \right], \quad (20)$$

and

$$\frac{d\sigma}{dt} = \frac{2}{\mu} \sum_k P_k \sum_{n=0}^k \left[(1-x) \left(\frac{n}{k} \right)^q g_{n,k}^+ B_-(n|k) - x \left(\frac{k-n}{k} \right)^q g_{n,k}^- B_+(n|k) \right] (k-2n). \quad (21)$$

Here P_k is the degree distribution of the graph, and μ is the mean degree. The quantity $B_\pm(n|k)$ is the probability that a type A/B node, which has degree k , has n neighbours of type A . Under the pair approximation this is a binomial distribution (see SM, Sec. S4).

In Fig. 7 we show the average fraction of agents of type A as a function of time for different graphs of varying average degree and for different values of q . The upper three panels are for degree-regular graphs, and as the data shows the pair approximation captures simulation results well, even quantitatively. Deviations are seen for Barabási-Albert and Erdős-Rényi graphs, in particular for $q = 2$ (the largest value of q shown in the figure). The pair approximation correctly predicts the convergence to $x = 1$, but the speed of the approach is underestimated, in

particular for smaller mean degrees, where the pair approximation is known to breakdown [34].

Overall, Fig. 7 demonstrates that the structure of the network affects the dynamics. In the examples shown, the effects of the mean degree are limited to intermediate times for $q \geq 1$ for all graphs we have tested. This is because in the long-run the system fixates $x = 1$, and the stability of this state is not affected in the range of mean degrees tested in Fig. 7. It is interesting to note that the dynamics in the pair-approximation can have multiple stable fixed points. We find this to be the case for $q > 2$ (see Fig. S4 in the SM, indicating co-ordination-type behaviour). Convergence to $x = 1$ is then only seen for some initial conditions.

The long-term average density of type A agents itself is affected for $q < 1$ (left-hand panels in Fig. 7). We note that the stationary density is here strictly between zero and one. Changes of the mean degree then directly alter the location of this fixed point of Eqs. (20) and (21).

The main purpose of this section was to describe how the pair approximation can be extended to q -deformed game dynamics. We stress again that the focal agent in our setup compares its current expected payoff to that it would receive if it were to change strategy. This is at variance with some existing studies of game dynamics on networks, where interaction only occurs with one single neighbour ($q = 1$) [35]. If there is only one interaction partner, it is perhaps natural to compare the payoffs of the focal node and that of the interaction partner. However, for $q > 1$, the focal node interacts with multiple other agents, so that payoff comparison with one single neighbour does not seem sensible. As an alternative to our dynamics one could consider a model in which the focal agent compares its current payoff to the average payoff of q neighbours (but again changes can only occur provided these neighbours are all of the same type). While we expect that the pair approximation can be developed also in such a scenario, we have not pursued this here. The main reason is that the resulting theory would become more cumbersome, as the evaluation of the functions $g_{n,k}^\pm$ is then no longer local, but would also have to be based on the payoffs of the neighbours of the focal node, which in turn will depend on the degrees of those neighbours, and the states of the neighbours of the neighbours.

VI. Multi-strategy cyclic games

A. q -deformed dynamics for multi-strategy games

We now consider games with $S > 2$ strategies, writing A_{ab} for the payoff that an agent playing strategy a receives when playing against an agent using strategy

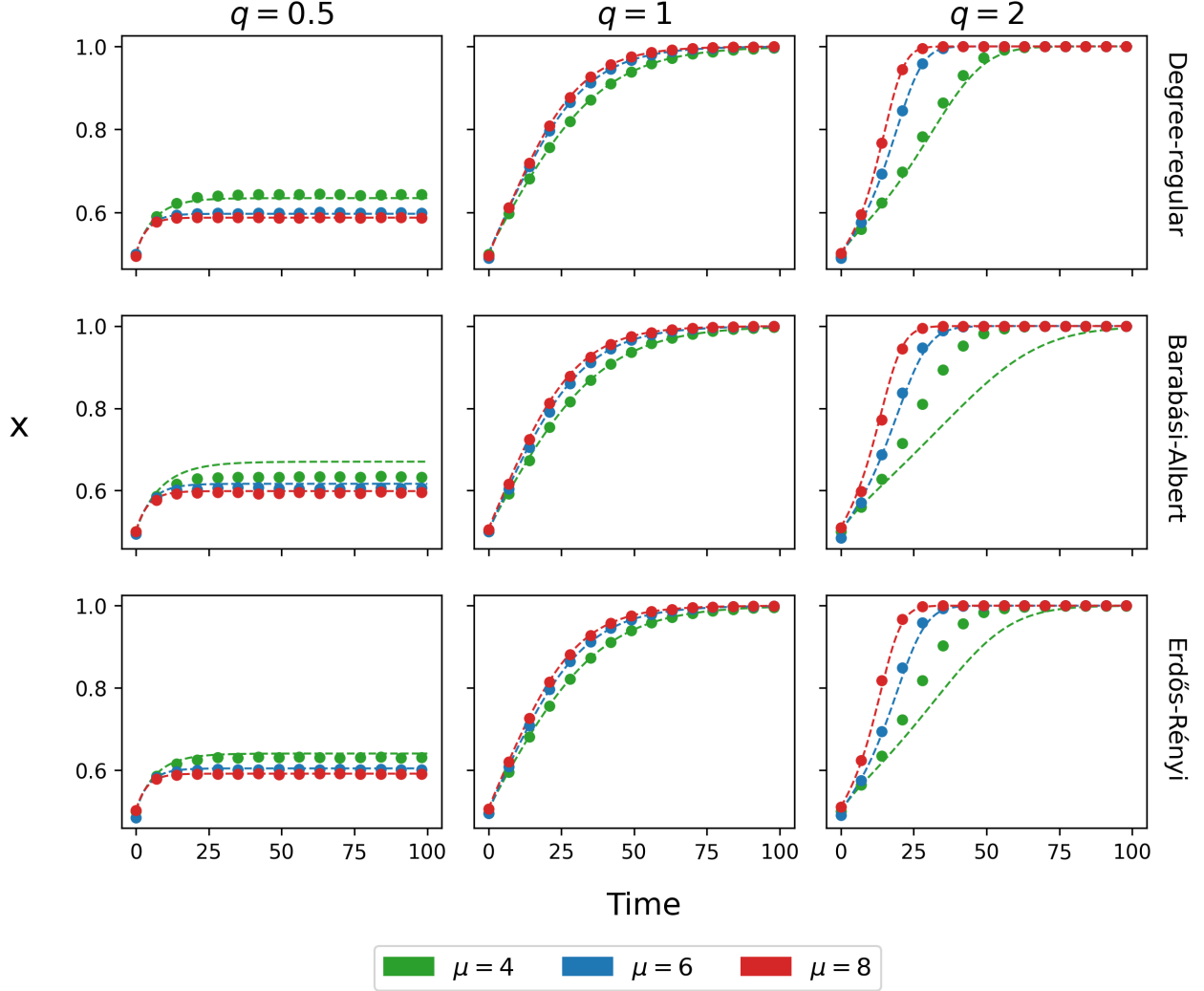


FIG. 7. Density of type A agents, x , as a function of time on various graphs with different average degree, μ , for different values of q . Dashed lines are the analytical results from numerically integrating Eqs. (S37a) and (S37b). Markers are results from averaging over 100 independent trajectories. The graphs in our simulations have size $N = 10,000$, and average degree as shown. The indicated average degrees can be generated exactly for degree-regular and Barabási-Albert graphs but only approximately for Erdős-Rényi graphs. The game parameters are $u = 0.1$ and $v = 0.1$.

b . We also write x_a for the proportion of individuals in the population playing strategy a , and introduce the column vector $\mathbf{x} = (x_1, \dots, x_S)^T$, where T stands for transpose. We have $\sum_{a=1}^S x_a = 1$. The average payoff of strategy a is then

$$\pi_a(\mathbf{x}) = \sum_b A_{ab} x_b. \quad (22)$$

We focus on populations with all-to-all interactions. The individual-based process is as before. We choose one individual at random for potential update, say this individual is of type a . In a second step q individuals are sampled from the population (with replacement). Only if all of these individuals are of the same type (which we will call b) can a change of the original type a individual occur. If this is the case,

the update from a to b is implemented with probability $g_{a \rightarrow b}(\mathbf{x})$.

The rate for changes from a to b is then

$$T_{a \rightarrow b} = N x_a x_b^q g_{a \rightarrow b}(\mathbf{x}), \quad (23)$$

where we use the Fermi function and define, similar to Eq. (6),

$$g_{a \rightarrow b}(\mathbf{x}) = \frac{1}{1 + e^{-\beta[\pi_a(\mathbf{x}) - \pi_b(\mathbf{x})]}}. \quad (24)$$

As in Sec. III we use these rates to obtain equations which govern the dynamics of the average density of type a agents in infinite populations. We find

$$\dot{x}_a = x_a^q \sum_{b \neq a} x_b g_{b \rightarrow a}(\mathbf{x}) - x_a \sum_{b \neq a} x_b^q g_{a \rightarrow b}(\mathbf{x}). \quad (25)$$

In the case of two strategies, we recover Eq. (8).

B. Three-strategy cyclic games

As an example we consider cyclic games with three pure strategies. This generalises the well-known rock-paper-scissors (RPS) game. Following [36, 37] we use the payoff matrix

$$\begin{array}{ccc} R & P & S \\ R & 0 & -1 & 1+\delta \\ P & 1+\delta & 0 & -1 \\ S & -1 & 1+\delta & 0 \end{array}, \quad (26)$$

where δ is real-valued. There are then two main model parameters, δ and q . Our notation follows that of [36], we note that a different parametrisation is used for example in [37]. In the SM (Sec. S5) we also analyse a more general two-parameter family of payoff matrices. We focus mostly on the case $\delta > -1$, such that the payoff to strategy ‘scissors’ for example is positive when playing against ‘paper’. Each pure strategy then beats one other pure strategy, and is beaten by the remaining pure strategy. The case $\delta \leq -1$ can also be analysed, but the game is then not a *bona fide* cyclic game.

The centre of the strategy simplex $(\frac{1}{3}, \frac{1}{3}, \frac{1}{3})$ is a fixed point of the dynamics for all q and δ , indicating co-existence of all three strategies. The monomorphic states at the corners are also fixed points (only one type of strategy survives). Performing a linear stability analysis (see SM, Sec. S5) we find that the co-existence fixed point is linearly stable if and only if

$$q < q_c(\delta) \equiv 1 + \frac{\delta}{6}. \quad (27)$$

The eigenvalues are complex for all $\delta \neq -1$, and thus the fixed point is a spiral sink for $q < q_c$, and a spiral source for $q > q_c$. When $q = q_c$ the fixed point is a centre.

A linear stability analysis of the corners show that these are stable (with two real-valued eigenvalues) for $q > 1$. For $q < 1$ the leading order-terms in the rate equations are sub-linear near the corners, and linear stability analysis does not apply. Nonetheless, the corners can be seen to be sources. When $q = 1$ the corners are saddle points for all $\delta > -1$. Section S5 in the SM contains further details.

For $q = 1$ the above payoff matrix is known to show different dynamics depending on the value of δ [36, 37]. For $\delta > 0$ trajectories spiral to the centre of the strategy simplex, i.e. the densities of all strategies tend to $\frac{1}{3}$. When $\delta = 0$ we have neutrally stable cyclic orbits around the central fixed point. For $-1 < \delta < 0$ one finds heteroclinic cycles, where the trajectories orbit near the edge of the simplex. For completeness

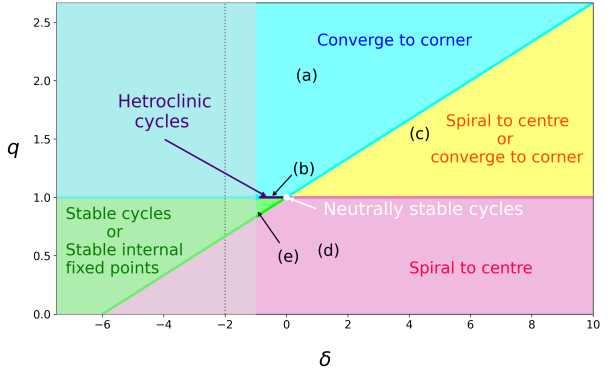


FIG. 8. Types of behaviour of the deterministic rate equations for the 3-strategy cyclic game using the payoff matrix in Eq. (26) as a function of q and δ . We mostly consider $\delta > -1$. The region $\delta \leq -1$ is also shown but greyed out. Blue: trajectories converge to one of the corners depending on initial conditions. Pink: trajectories spiral to centre point for all initial conditions. Green: trajectories converge to the same limit cycle [one for each (q, δ) pair] for all initial conditions, or trajectories can converge to stable internal fixed points within the simplex that are not the centre or corners. Indigo: trajectories converge to heteroclinic cycles on the edges of the simplex for all initial conditions. Yellow: depending on the initial conditions, trajectories will either spiral to the centre or converge to one of the corners. White: trajectories perform neutrally stable cycles for all initial conditions. By initial conditions we mean that the trajectories start from a point in the simplex that is not the centre or one of the corners. We include a faint dotted grey line at $\delta = -2$ for reference. The annotations in the plot correspond to the ternary diagrams in Fig. 9. $(q, \delta) = [(2, 0.3), (1, -0.5), (1.5, 4), (0.5, 1), (0.87, -0.95)]$ for (a)-(e) respectively. The diagram is constructed from analysing the stability of the central fixed points and the corners, together with numerical integration of the rate equations. As a caveat we add that we cannot exclude the existence of further fixed points (see also SM, Sec. S5).

we remark that the corners of the strategy simplex are stable fixed points when $\delta \leq -1$ and $q = 1$. One then finds convergence to the corners.

In Fig. 8 we show a phase diagram in the (q, δ) -plane highlighting the different types of outcome for the cyclic 3-strategy game for different q and δ . We emphasise that the behaviour in the different phases is determined from the stability analysis of the corners and the centre, combined with numerical exploration of the q -deformed rate equations. We cannot exclude the possibility of further fixed points in the interior, or on the edges of the simplex (see also SM, Sec. S5D). Subject to this disclaimer, we find that q -deformation can generate new types of flow, which we will now describe in turn.

When $\delta > 0$ and $1 < q < q_c(\delta)$ (yellow region in Fig. 8) the dynamics either spirals to the centre or converges to one of the corners, depending on initial

conditions. For $q > \max\{1, q_c(\delta)\}$, $q = q_c(\delta)$ with $\delta > 0$, or $q = 1$ with $\delta \leq -1$, (cyan region, including the cyan lines) we find convergence to one of the corners, which corner depends again on initial conditions. For $\delta < 0$ and $q_c(\delta) \leq q < 1$ (green region, including the green line), we either have stable limit cycles or trajectories converge to stable internal fixed points that are not the centre or the corners. The latter tends to occur for $\delta \approx -2$, an example is given in SM, Sec. S5 D. In the indigo region ($q = 1, -1 < \delta < 0$) the system shows heteroclinic cycles. For $q = 1, \delta = 0$ (white point in the diagram) one finds neutrally stable cycles. Finally for $q < \min\{1, q_c(\delta)\}$, or $q = 1$ with $\delta > 0$, (pink region, including the pink line) the dynamics spirals to the centre. For completeness we have included some range of $\delta \leq -1$ in Fig. 8, even if the payoff matrix there does not describe a *bona fide* cyclic game. $\delta = -2$ is a special case where the centre is a stable/unstable star (see SM, Sec. S5 D).

In Fig. 9 we illustrate these different types of flow in the strategy simplex. The choice for (q, δ) are as annotated in Fig. 8.

VII. q -deformed dynamics without replacement

Until now we have always assumed that the q neighbours of the focal agent are chosen with replacement

(i.e. the same individual can be chosen more than once). In this section, we focus on the case without replacement. It now only makes sense to consider integer values of q . We focus on 2-strategy 2-player games and populations with all-to-all interaction. The state of the population is then fully described by the number i of individuals playing strategy A .

The rates for the events $i \rightarrow i \pm 1$ in the model without replacement are

$$T_i^+ = \begin{cases} 0, & 0 \leq i < q \\ (N-i)g_i^+ \prod_{k=1}^q \left(\frac{i-k+1}{N-k}\right), & q \leq i \leq N \end{cases} \quad (28a)$$

$$T_i^- = \begin{cases} ig_i^- \prod_{k=1}^q \left(\frac{N-i-k+1}{N-k}\right), & 0 \leq i \leq N-q \\ 0, & N-q < i \leq N \end{cases} \quad (28b)$$

respectively, where we have defined $g_i^\pm \equiv g^\pm(i/N)$. We have $T_i^+ = 0$ for $i < q$, this is because there must be at least q type A agents in the system in order for a type B agent to select q type A other agents without replacement. Similarly $T_i^- = 0$ for $i > N-q$. More detail on these rates can be found in Sec. S6 of the SM.

Given the rates in Eqs. (28a) and (28b) we derive the fixation probability to be (see again Sec. S6 in the SM):

$$\phi_i = \begin{cases} 0, & (q \leq \frac{N}{2} \text{ and } 0 \leq i < q) \text{ or } (q > \frac{N}{2} \text{ and } 0 \leq i < q), \\ \frac{\sum_{k=q}^i \prod_{j=q}^{k-1} \gamma_j}{\sum_{k=q}^{N-q+1} \prod_{j=q}^{k-1} \gamma_j}, & q \leq \frac{N}{2} \text{ and } q \leq i \leq N-q, \\ 1, & (q \leq \frac{N}{2} \text{ and } N-q < i \leq N) \text{ or } (q > \frac{N}{2} \text{ and } q \leq i \leq N). \end{cases} \quad (29)$$

Here $\gamma_j = T_i^-/T_i^+$ with T_i^\pm as in Eqs. (28a) and (28b). The fixation probabilities are better illustrated in (i, q) -space, as shown in Fig. 10 for different choices of u and v . The interesting region is that defined by the middle condition of Eq. (29) as this is the only region where the fixation probability depends on the game (in the other two regions, the fixation probability is zero or one respectively, independent of u and v). We highlight this in Fig. 10, the region of interest is that in the triangle on the left of each panel.

In Fig. 10(a) the fixation probability is very close to one in this area. Since u and v are large in panel (a) this would typically be an A -dominance game (see Fig. 2). At the other extreme (u and v sufficiently negative) the flow is mostly of the B -dominance type [Fig. 10(d)], and in the region of interest the fixation probability is very close to zero. For intermediate values of u and v the region of interest divides non-trivially into two areas, one in which ϕ_i is close to

one, and another in which the fixation probability is close to zero [panels (b) and (c)].

VIII. Discussion

In summary, we have combined ideas from the non-linear q -voter model with dynamics in evolutionary game theory. The q -voter model was originally introduced as a non-linear extension of the conventional voter model, and with a view towards understanding how non-linearity affects the statistical physics of simple systems with absorbing states. Evolutionary game dynamics is non-linear by itself, thus the goal of this work was to study how additional q -deformation affects the outcome both in infinite and in finite populations. For integer q there is a clear interpretation of the dynamics: an agent in the population consults with q other agents. If all those other agents are in a

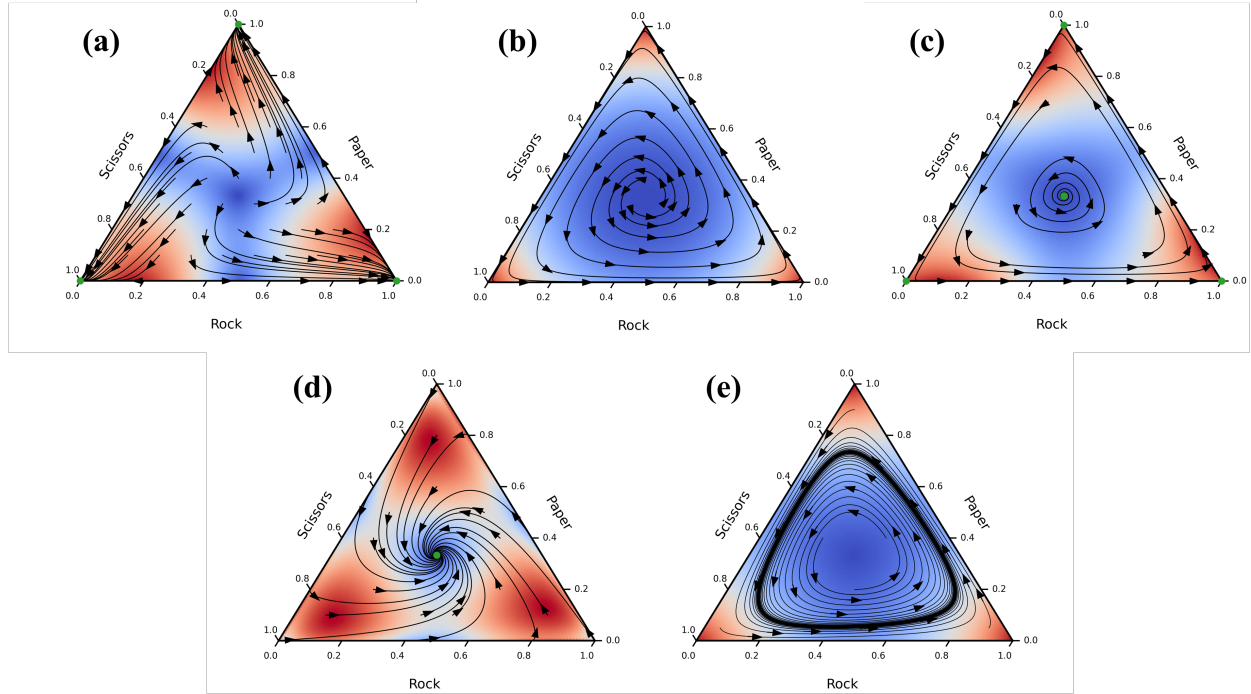


FIG. 9. Ternary plots for the 3-strategy cyclic game defined by the payoff matrix in Eq. (26) for different values of (q, δ) as annotated in Fig. 8. Green points are sinks. The background colour indicates the speed with which the trajectories move in the simplex, hotter colours are faster. The lines of constant x_i are parallel to the tick marks on edge labelled $i \in \{\text{Rock}, \text{Paper}, \text{Scissors}\}$. For example, lines of constant x_{paper} are horizontal.

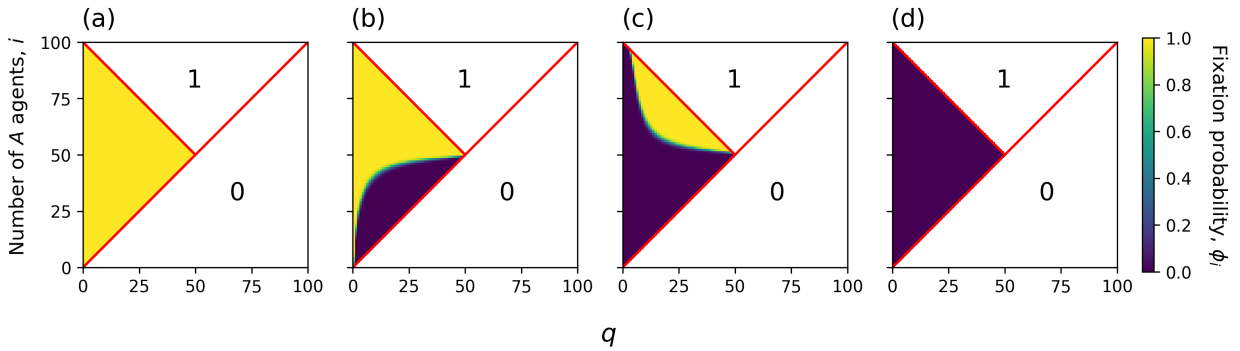


FIG. 10. Fixation probability for the q -deformed dynamics without replacement, Eq. (29), in the (q, i) -plane. This is for a population with $N = 100$ for different game parameters, namely $(u, v) = [(10, 10), (0.1, -0.03), (-0.1, -0.1), (-1, -1)]$ from left to right. There are two white regions, annotated with 0 and 1, where the fixation probability is given by those values. These regions correspond to cases one and three of Eq. (29). In the coloured region [case two of Eq. (29)], the fixation probability is often extremely close to 0 (purple) or 1 (yellow), but we stress that it does not take these values exactly.

state which is different from that of the focal agent, that latter agent considers a change of strategy. This is then implemented with a probability based on payoff gain. Mathematically, the model can be studied for any real-valued q .

As we have seen, the combination of q -deformation and selection because of the underlying game can produce a number of new types of flow, not seen in conventional game dynamics ($q = 1$). In 2×2 games multiple internal fixed points become possible, thus

generating scenarios such as bi-stable co-existence or mixed co-existence and co-ordination. We have systematically studied where in the space of games these different cases occur, as q is varied. In cyclic games with three strategies one also finds dynamics which are not possible without q -deformation, notably stable limit cycles and deterministic flow converging to pure-strategy points. We also find cases with multiple attracting fixed points in the interior of the strategy simplex (Sec. S5D). Finally, we have shown how fix-

ation times and probabilities can be calculated for q -deformed dynamics in finite populations, and we have extended pair approximation methods for interacting agents on networks to q -deformed processes.

The main purpose of this paper is to introduce the general idea of q -deformation in game dynamics, to study a number of basic scenarios and to put the relevant tools in place. There are a number of lines which could be pursued in future work. For example, it might be interesting to see how q -deformation affects the ordering dynamics of evolutionary games on regular lattices. One might expect departures from the universality class of directed percolation for example [35]. Similarly, one could study more systematically how the system departs from the q -voter model in the limit of weak selection.

More generally, changing the strength of selection in an evolving population can have surprising effects. For example, so-called ‘stochastic slowdown’ has been reported [38], that is the conditional fixation time of a mutant can decrease even if the selective advantage of the mutant is increased. Non-monotonic behaviour of the conditional fixation time as a function of selection strength has also been observed [39]. Our analysis has shown that q -deformation also affects fixation times. It would be interesting to investigate if effects similar to stochastic slowdown also occur. We note that q -deformation not only changes the strength of evolutionary flow but also the location of co-existence fixed points. This is not the case in [38, 39], where the position of fixed points remain the same as the strength of selection is changed.

Further aspects for future work might include multi-player games (e.g. public-good games), or asking if and how q -deformation affects the tendency of specific graphs to act as amplifiers or suppressors of selection [11, 40].

Acknowledgements

This work was supported by the the Agencia Estatal de Investigación and Fondo Europeo de Desarrollo Regional (FEDER, UE) under project APASOS (PID2021-122256NB-C21, PID2021-122256NB-C22), the María de Maeztu programme for Units of Excellence, CEX2021-001164-M funded by MCIN/AEI/10.13039/501100011033. We also acknowledge a studentship by the Engineering and Physical Sciences Research Council (EPSRC, UK), reference EP/T517823/1.

— Supplemental Material —

Contents

S1. Deriving the q -deformed rate equations	S1
S2. Classifying 2×2 q -deformed evolutionary dynamics	S2
A. Fixed points and stability	S2
B. Phase diagram	S4
1. General analysis	S4
2. The limit $q \rightarrow \infty$	S5
3. Large, but finite q	S5
4. The limit $q \rightarrow 0$	S6
S3. Fixation probability and fixation time for 2×2 games with q -deformed dynamics	S6
A. Fixation probability	S6
B. Fixation time	S7
C. Further results for the system in Figs. 5 and 6	S8
S4. Pair approximation on graphs	S8
A. Notation	S8
B. Rate of change of the proportion of agents of type A	S9
C. The homogeneous pair approximation	S9
D. Rate of change of σ	S10
E. Transition rates on graphs	S10
F. Analytically tractable limits	S11
1. Voter model limit	S11
2. Complete graph limit	S12
G. Degree-regular graphs	S12
H. Non-regular graphs	S13
S5. q -deformed dynamics for cyclic games	S14
A. The centre point	S15
B. The corners	S15
1. $q = 1$	S15
2. $q > 1$	S16
3. $0 < q < 1$	S16
C. Reduction to one-parameter family of payoff matrices	S16
D. Further ternary plots	S17
S6. Fixation probability for q -deformed dynamics without replacement for 2×2 games	S17
References	S19

S1. Deriving the q -deformed rate equations

We focus on a well-mixed population of size N , and a game with two pure strategies. Define $P(x; t)$ as the probability for the system to be in state $x = i/N$ at time t , where i is the number of type A individuals. Given that the dynamics can be described via the rates $T^+(x)$ and $T^-(x)$, which increase/decrease x by $\frac{1}{N}$ respectively, the master equation can be written

$$\frac{d}{dt} P(x; t) = P\left(x - \frac{1}{N}, t\right) T^+ \left(x - \frac{1}{N}\right) + P\left(x + \frac{1}{N}, t\right) T^- \left(x + \frac{1}{N}\right) - P(x, t) T^+(x) - P(x, t) T^-(x). \quad (\text{S1})$$

From this, the first moment $\langle x(t) \rangle$, which is the average density of type A agents, has the following differential equation,

$$\begin{aligned}
\frac{d\langle x(t) \rangle}{dt} &= \sum_x x \left[P\left(x - \frac{1}{N}, t\right) T^+ \left(x - \frac{1}{N}\right) + P\left(x + \frac{1}{N}, t\right) T^- \left(x + \frac{1}{N}\right) \right] \\
&\quad - \sum_x x P(x, t) [T^+(x) + T^-(x)] \\
&= \sum_x \left(x - \frac{1}{N}\right) P(x, t) T^+(x) + \sum_x \left(x + \frac{1}{N}\right) P(x, t) T^-(x) \\
&\quad - \langle x T^+(x) \rangle - \langle x T^-(x) \rangle \\
&= \langle x T^+(x) \rangle - \frac{1}{N} \langle T^+(x) \rangle + \langle x T^-(x) \rangle - \frac{1}{N} \langle T^-(x) \rangle - \langle x T^+(x) \rangle - \langle x T^-(x) \rangle \\
&= \frac{1}{N} [\langle T^+(x) \rangle + \langle T^-(x) \rangle]. \tag{S2}
\end{aligned}$$

Assuming the population is of infinite size, we can ignore fluctuations. This means that the probability distribution $P(x; t)$, i.e. the solution to the master equation in Eq. (S1), is concentrated on its mean,

$$P(x, t) \rightarrow P(x, t) = \delta(x - \langle x(t) \rangle). \tag{S3}$$

With this we can simplify the average rates that appear in Eq. (S2),

$$\langle T^\pm(x) \rangle = \int T^\pm(x) P(x, t) dx = \int T^\pm(x) \delta(x - \langle x(t) \rangle) dx = T^\pm(\langle x(t) \rangle). \tag{S4}$$

We ease the notation by writing $\langle x(t) \rangle$ as just x , thus we have

$$\frac{dx}{dt} = \frac{1}{N} [T^+(x) - T^-(x)]. \tag{S5}$$

We can then use the rates from Eq. (7) to get the ‘ q -deformed’ dynamics in Eq. (8).

S2. Classifying 2×2 q -deformed evolutionary dynamics

To classify the outcome of q -deformed dynamics for 2×2 games we determine all fixed points, x^* , and their stability.

A. Fixed points and stability

The fixed points are obtained by setting the right-hand side of Eq. (8) to zero,

$$(1 - x^*)(x^*)^q g^+(x^*) - x^*(1 - x^*)^q g^-(x^*) = 0. \tag{S6}$$

Of course $x^* = 0, 1$ are trivial solutions corresponding to fixed points on the boundaries. We will determine their stability below. To find the interior fixed points we define

$$f(x) = \ln \left(\frac{x}{1 - x} \right) - \frac{1}{q - 1} \frac{g^+(x)}{g^-(x)}, \tag{S7}$$

assuming $x \neq 0, 1$. The solutions to $f(x^*) = 0$ would give all interior fixed points. However, this is a non-linear equation with no analytic solution in general. Despite this, it is still possible to determine the dynamics for some given function g .

We assume that g takes the form of the Fermi function, as in Eq. (6). Equation (S7) then becomes

$$f_{\text{Fermi}}(x) = \ln \left(\frac{x}{1 - x} \right) - \frac{1}{1 - q} (ux + v). \tag{S8}$$

This function only exists in the interval $x \in (0, 1)$. We find

$$\lim_{x \rightarrow 0^+} f_{\text{Fermi}}(x) \rightarrow -\infty, \quad (\text{S9a})$$

$$\lim_{x \rightarrow 1^-} f_{\text{Fermi}}(x) \rightarrow +\infty. \quad (\text{S9b})$$

Since $f_{\text{Fermi}}(x)$ is a continuous function there must therefore be at least one zero, so there is always at least one interior fixed point. The maximum number of zeroes is determined by the number of stationary points (extrema) of $f_{\text{Fermi}}(x)$, alongside the signs of $f_{\text{Fermi}}(x)$ at those stationary points. For example, if there are two stationary points and if $f_{\text{Fermi}}(x)$ takes a positive value at one of these point, and a negative value at the other, then $f_{\text{Fermi}}(x)$ has three zeroes, and hence there are three interior fixed points.

Differentiating Eq. (S8) and equating to zero gives the quadratic equation

$$x^2 - x + \frac{1-q}{u} = 0, \quad (\text{S10})$$

which has solutions

$$x_{1,2} = \frac{1}{2} \left[1 \pm \sqrt{1 - 4 \frac{1-q}{u}} \right]. \quad (\text{S11})$$

These are the locations of the stationary points of the function $f_{\text{Fermi}}(x)$ in Eq. (S8). Thus, depending on the values of the parameters q and u , we can have zero, one or two stationary points.

The possible scenarios are as follows:

- (i) $\frac{1-q}{u} > \frac{1}{4}$, $f_{\text{Fermi}}(x)$ has no stationary points. Thus $f_{\text{Fermi}}(x)$ has one zero, meaning there is one interior fixed point.
- (ii) $\frac{1-q}{u} = \frac{1}{4}$, $f_{\text{Fermi}}(x)$ has one stationary point at $x^* = \frac{1}{2}$, so $f_{\text{Fermi}}(x)$ has one zero, and there is one interior fixed point.
- (iii) $0 < \frac{1-q}{u} < \frac{1}{4}$, $f_{\text{Fermi}}(x)$ has two stationary points, x_1 and x_2 , both of which are in the interval $x \in (0, 1)$. This leads to the following sub-scenarios:
 - (a) The two stationary points have opposite signs, i.e. $f_{\text{Fermi}}(x_1) \cdot f_{\text{Fermi}}(x_2) < 0$, which means $f_{\text{Fermi}}(x)$ has three zeroes, hence there are three interior fixed points.
 - (b) The two stationary points have the same sign, i.e. $f_{\text{Fermi}}(x_1) \cdot f_{\text{Fermi}}(x_2) > 0$, which means $f_{\text{Fermi}}(x)$ has one zero, and hence there is one interior fixed point.
 - (c) One stationary point lies exactly on the axis $f_{\text{Fermi}}(x) = 0$, i.e. either $f_{\text{Fermi}}(x_1) = 0$ or $f_{\text{Fermi}}(x_2) = 0$, which means $f_{\text{Fermi}}(x)$ crosses the horizontal axis once and touches it once at another location. Hence, there are two interior fixed points.
- (iv) $\frac{1-q}{u} \leq 0$, Eq. (S11) has two solutions but they lie outside of the range $x \in (0, 1)$. Since $f_{\text{Fermi}}(x)$ is bounded on $x \in (0, 1)$ these are not valid solutions. Thus $f_{\text{Fermi}}(x)$ has no stationary points, which means it crosses the x -axis once, so one interior fixed point.

Next we determine the stability of the boundary fixed points. If $q > 1$, then $f_{\text{Fermi}}(x)$ and $\dot{x} = \frac{dx}{dt}$ will always be both greater than zero or both less than zero. For $q < 1$ one will be greater than zero and the other less than zero. This can be easily proved by first assuming $\dot{x} > 0$ [Eq. (S6)]. Then manipulate the inequality into the form of Eq. (S8), at which point we find $f_{\text{Fermi}}(x) > 0$ (if $q > 1$) or $f_{\text{Fermi}}(x) < 0$ (if $q < 1$), i.e. the same/opposite sign to \dot{x} .

Now, we know from Eq. (S9a) that $f_{\text{Fermi}}(x)$ is negative as $x \rightarrow 0^+$, thus for $q > 1$, \dot{x} will also be negative in this limit. This means that the fixed point at $x^* = 0$ is stable. We can use a similar argument to show that the fixed point at $x^* = 1$ is also stable.

The stability of the interior fixed points can be determined in the same way. For example, if \dot{x} and $f_{\text{Fermi}}(x)$ have the same sign, and $f_{\text{Fermi}}(x)$ only crosses the horizontal axis [$f_{\text{Fermi}}(x) = 0$] once, there is one interior fixed point, and that fixed point must be unstable.

Discriminant classification	Stationary point value	value of q	Classification
$\frac{1-q}{u} \geq \frac{1}{4}$ or $\frac{1-q}{u} \leq 0$	N/A	$q > 1$	Co-ordination
		$q < 1$	Co-existence
$0 < \frac{1-q}{u} < \frac{1}{4}$	$f_{\text{Fermi}}(x_1) \cdot f_{\text{Fermi}}(x_2) > 0$	$q > 1$	Co-ordination
		$q < 1$	Co-existence
	$f_{\text{Fermi}}(x_1) \cdot f_{\text{Fermi}}(x_2) < 0$	$q > 1$	Mixed co-ordination/co-existence
		$q < 1$	Bi-stable co-existence
	$f_{\text{Fermi}}(x_1) = 0$	$q > 1$	Marginally bi-stable co-ordination
		$q < 1$	Marginally bi-stable co-existence
	$f_{\text{Fermi}}(x_2) = 0$	$q > 1$	Marginally bi-stable co-ordination
		$q < 1$	Marginally bi-stable co-existence

TABLE S1. Classification of Eq. (8) depending on the various parameters chosen. The first column evaluates the discriminant of Eq. (S10) to determine the number of stationary points of $f_{\text{Fermi}}(x)$, Eq. (S8). The second column evaluates $f_{\text{Fermi}}(x)$ at the stationary points, x_1 and x_2 given by Eq. (S11), where we assume $x_1 < x_2$, to determine the number of x -axis crosses. The third column differentiates between $q > 1$ and $q < 1$. The fourth column then gives the classification of the game.

The above classifications are summarised in Tab. S1. Graphical representations of these classifications are shown in Fig. 3. We note that there are four scenarios that lead to ‘marginally bi-stable’ flow. These types of flow are rare in comparison to the others. We group the classifications into two pairs: ‘marginally bi-stable co-existence’ and ‘marginally bi-stable co-ordination’. The difference within a pair is the ordering of the two interior fixed points.

B. Phase diagram

1. General analysis

These classifications are better illustrated by a phase plot in the (u, v) -plane, which will also help to highlight how the q -deformed flow changes as we alter the payoff matrix. We first want to determine all points in the (u, v) -plane that would give marginally bi-stable flow. To do this we substitute the stationary point solutions x_1 and x_2 , given by Eq. (S11), into $f_{\text{Fermi}}(x)$ [Eq. (S8)], then set this equal to zero and solve. This is equivalent to solving $f_{\text{Fermi}}(x_{1,2}) = 0$ which, as seen from Tab. S1, is what defines marginally bi-stable flow. We find

$$v^{(1)} = (1-q) \ln \left(\frac{x_1}{1-x_1} \right) - ux_1, \quad (\text{S12a})$$

$$v^{(2)} = (1-q) \ln \left(\frac{x_2}{1-x_2} \right) - ux_2. \quad (\text{S12b})$$

Recall from Eq. (S11) that $x_{1,2}$ are functions of q and u , thus for a given value of q , Eqs. (S12a) and (S12b) are lines in the (u, v) -plane. These equations are only valid for $q > 1$ when $-\infty < u \leq \tilde{u}$, and for $q < 1$ when $\tilde{u} \leq u < \infty$, where

$$\tilde{u} = 4(1-q). \quad (\text{S13})$$

Otherwise Eq. (S11) does not have real solutions.

Along the line defined by $v^{(1)}$ one has $f_{\text{Fermi}}(x_1) = 0$, i.e. marginally bi-stable co-ordination and marginally bi-stable co-existence for $q > 1$ and $q < 1$ respectively. Similarly, sitting on the $v^{(2)}$ line corresponds to $f_{\text{Fermi}}(x_2) = 0$, again marginally bi-stable co-ordination and marginally bi-stable co-existence for $q > 1$ and $q < 1$ respectively. The region between these lines corresponds to $f_{\text{Fermi}}(x_1) \cdot f_{\text{Fermi}}(x_2) < 0$, i.e. mixed co-ordination/co-existence or bi-stable co-existence for $q > 1$ and $q < 1$ respectively. The region outside of these lines is simply standard co-ordination or co-existence for $q > 1$ and $q < 1$ respectively.

Fig. S1 demonstrates the idea for different values of q . This figure highlights the fact that marginally bi-stable co-ordination and marginally bi-stable co-existence type flow are rare, as they are only seen on well defined lines in the (u, v) -plane. Most of the time we see either co-ordination/co-existence, or mixed co-ordination/co-existence ($q > 1$) and bi-stable co-existence ($q < 1$).

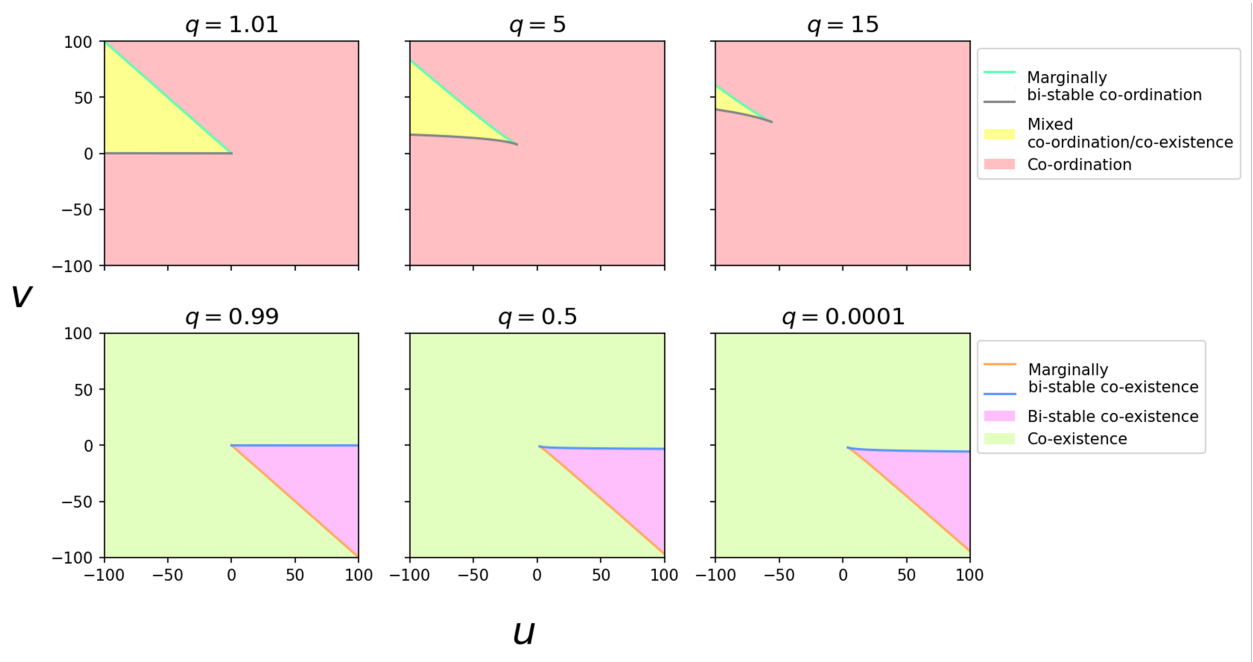


FIG. S1. Phase plots in (u, v) -space showing how the classification regions of the q -deformed replicator equations change as we alter the payoff matrix for different q . Regions are coloured in line with Figs. 1 and 3 in the main paper.

2. The limit $q \rightarrow \infty$

In the limit $q \rightarrow \infty$ both $(1 - x)^q$ and x^q go to zero for any $0 < x < 1$. Thus Eq. (S6) is satisfied for all values of $x \in (0, 1)$, meaning all such points are fixed points. This is because for $q \rightarrow \infty$ no events can occur in a population containing individuals both of type A and type B .

3. Large, but finite q

For large but finite q , the mixed co-ordination/co-existence region shrinks and standard co-ordination dominates due to the fact that \tilde{u} becomes large and negative [see Eq. (S13)], which is the upper bound for u for the mixed co-ordination/co-existence region. The interior fixed point of the dominating co-ordination region is $x^* \approx \frac{1}{2}$ at all points in the space classified as co-ordination. This can be seen by noting that as q becomes large

$$f_{\text{Fermi}}(x) \approx \ln\left(\frac{x}{1-x}\right), \quad (\text{S14})$$

and $\ln\left(\frac{x^*}{1-x^*}\right) = 0$ has one solution, namely $x^* = \frac{1}{2}$. So for large positive q we only get co-ordination type flow with $x^* \approx \frac{1}{2}$, and we conclude that $q > 1$ dynamics promotes the majority, i.e. if there are less A types than B types the dynamics drives the population of A types down to zero.

Since q is only large, but still finite, there always exists a region of mixed co-ordination/co-existence (yellow region in Fig. S1), but only for large negative u , and $v > 0$. This is because in the standard $q = 1$ case these mixed co-ordination/co-existence regions are co-existence regions [see Fig. 2]. The dynamics promotes the minority, i.e. if there are less A types the dynamics attempts to drive the number upwards. In this way, there is a balance between the the game itself favouring the minority, and the q -deformation for $q > 1$ promoting the majority. As we increase q , the influence of the q -deformation dominates, and the mixed co-ordination/co-existence region shrinks.

4. The limit $q \rightarrow 0$

In the limit $q \rightarrow 0$, the q -deformation favours co-existence. This time however, $\tilde{u} \rightarrow 4$ is a finite limit [see Eq. (S13)]. Thus there always exists a region of bi-stable co-existence (even for $q \rightarrow 0$), as seen in the lower panels of Fig. S1. The reasoning for this is analogous to that for large finite q : the q -deformed dynamics promotes the minority while the standard replicator flow ($q = 1$) in this region would promote the majority [see Fig. 2]. Decreasing q initially means the influence of the q -deformation increases, so co-existence starts to take over. However, past a certain point this effect diminishes, and decreasing q further results in no change.

S3. Fixation probability and fixation time for 2×2 games with q -deformed dynamics

A. Fixation probability

For an initial number of type A agents, i , we want to calculate the fixation probability ϕ_i , which is the probability for the system to reach the state $i = N$, i.e. all agents in the population are of type A .

It is well known that [10]

$$\phi_i = \frac{1 + \sum_{k=1}^{i-1} \prod_{j=1}^k \gamma_j}{1 + \sum_{k=1}^{N-1} \prod_{j=1}^k \gamma_j}, \quad (\text{S15})$$

where $\gamma_i = \frac{T_i^-}{T_i^+}$. Using the transition rates for our model, Eq. (7), we can write

$$\gamma_i = \left(\frac{N-i}{i} \right)^{q-1} \frac{g_i^-}{g_i^+}. \quad (\text{S16})$$

We note that $g_i^\pm \equiv g^\pm \left(\frac{i}{N} \right)$. Using the Fermi function as the choice for g^\pm [Eq. (6)], we can write the ratio

$$\frac{g_i^-}{g_i^+} = e^{-\Delta\pi_i}. \quad (\text{S17})$$

Thus we have

$$\gamma_i = \frac{T_i^-}{T_i^+} = \left(\frac{N-i}{i} \right)^{q-1} e^{-\Delta\pi_i}, \quad (\text{S18})$$

which can be interpreted as the tendency for the system to decrease the number of type A agents. Again, we define $\Delta\pi_i \equiv \Delta\pi \left(\frac{i}{N} \right)$, where $\Delta\pi(\cdot)$ is as in Eq. (3).

We now follow the lines of [30]. Equation (S15) requires evaluating the product

$$\begin{aligned} \prod_{j=1}^k \gamma_j &= \prod_{j=1}^k \left(\frac{N-j}{j} \right)^{q-1} e^{-\Delta\pi_j} \\ &= \left(\frac{N-1}{1} \right)^{q-1} e^{-\Delta\pi_1} \left(\frac{N-2}{2} \right)^{q-1} e^{-\Delta\pi_2} \dots \left(\frac{N-k}{k} \right)^{q-1} e^{-\Delta\pi_k} \\ &= \left(\frac{N-1}{1} \right)^{q-1} \left(\frac{N-2}{2} \right)^{q-1} \dots \left(\frac{N-k}{k} \right)^{q-1} \exp \left\{ - \sum_{j=1}^k \Delta\pi_j \right\} \\ &= \left[\frac{(-1)^k (1-N)_k}{k!} \right]^{q-1} \exp \left\{ - \sum_{j=1}^k \left(u \frac{j}{N} + v \right) \right\}, \end{aligned} \quad (\text{S19})$$

where $(\cdot)_k$ is the Pochhammer symbol [33] and we have used the formula for the payoff difference as in Eq. (3). The summation inside the exponential has a simple closed form which we will write as

$$\sum_{j=1}^k (u \frac{j}{N} + v) = \frac{k(k+1)}{2N} u + kv = H(k; u, v) \equiv H_k. \quad (\text{S20})$$

We also define the following function which appears in Eq. (S19) as

$$f_k \equiv f(k; N) = \frac{(-1)^k (1-N)_k}{k!}. \quad (\text{S21})$$

With this we can write the fixation probability as

$$\phi_i = \frac{1 + \sum_{k=1}^{i-1} f_k^{q-1} e^{-H_k}}{1 + \sum_{k=1}^{N-1} f_k^{q-1} e^{-H_k}}. \quad (\text{S22})$$

In the limit $q \rightarrow 1$, we recover the known formula for the standard Fermi process (with no deformation) [30, p; 5].

B. Fixation time

We want to calculate the unconditional, t_1 , and conditional, t_1^A , fixation times for q -deformed dynamics. t_1^A is the time it would take type A agents to take over the population, whereas t_1 is the time it would take for the type A agents to take over or become extinct, both starting from a single type A agent.

For general event rates of the one-step process these can be calculated as [10]

$$t_1 = \phi_1 \sum_{k=1}^{N-1} \sum_{\ell=1}^k \frac{1}{T_\ell^+} \prod_{m=\ell+1}^k \gamma_m, \quad (\text{S23a})$$

$$t_1^A = \sum_{k=1}^{N-1} \sum_{\ell=1}^k \frac{\phi_\ell}{T_\ell^+} \prod_{m=\ell+1}^k \gamma_m, \quad (\text{S23b})$$

where γ_k is the ratio of transition probabilities, given by Eq. (S18), and ϕ_ℓ is the probability to fixate from ℓ type A agents, given by Eq. (14). These equations can be written in a simpler form by evaluating the product, analogous to what was done in Sec. S3 A,

$$\begin{aligned} \prod_{m=\ell+1}^k \gamma_m &= \frac{\prod_{m=\ell}^k \gamma_m}{\prod_{m=\ell}^l \gamma_m} \\ &= \frac{f_k^{q-1} e^{-\beta H_k}}{f_\ell^{q-1} e^{-\beta H_\ell}} \\ &= \left(\frac{f_k}{f_\ell} \right)^{q-1} e^{-(H_k - H_\ell)}. \end{aligned} \quad (\text{S24})$$

Thus the fixation times can be written,

$$t_1 = \phi_1 \sum_{k=1}^{N-1} \sum_{\ell=1}^k \frac{1}{T_\ell^+} \left(\frac{f_k}{f_\ell} \right)^{q-1} e^{-(H_k - H_\ell)}, \quad (\text{S25a})$$

$$t_1^A = \sum_{k=1}^{N-1} \sum_{\ell=1}^k \frac{\phi_\ell}{T_\ell^+} \left(\frac{f_k}{f_\ell} \right)^{q-1} e^{-(H_k - H_\ell)}, \quad (\text{S25b})$$

where f_k and H_k are the functions defined in Eqs. (15) and (16) respectively.

C. Further results for the system in Figs. 5 and 6

Further results for the system in Figs. 5 and 6 can be found in Fig. S2. For $q \gtrsim 2.15$ the flow is of the co-ordination type. The figure shows that increasing q in this regime makes it more and more likely that the next event is towards the absorbing monomorphic states at $x = 0$ and $x = 1$. This reduces the probability for a single mutant to take over the population.

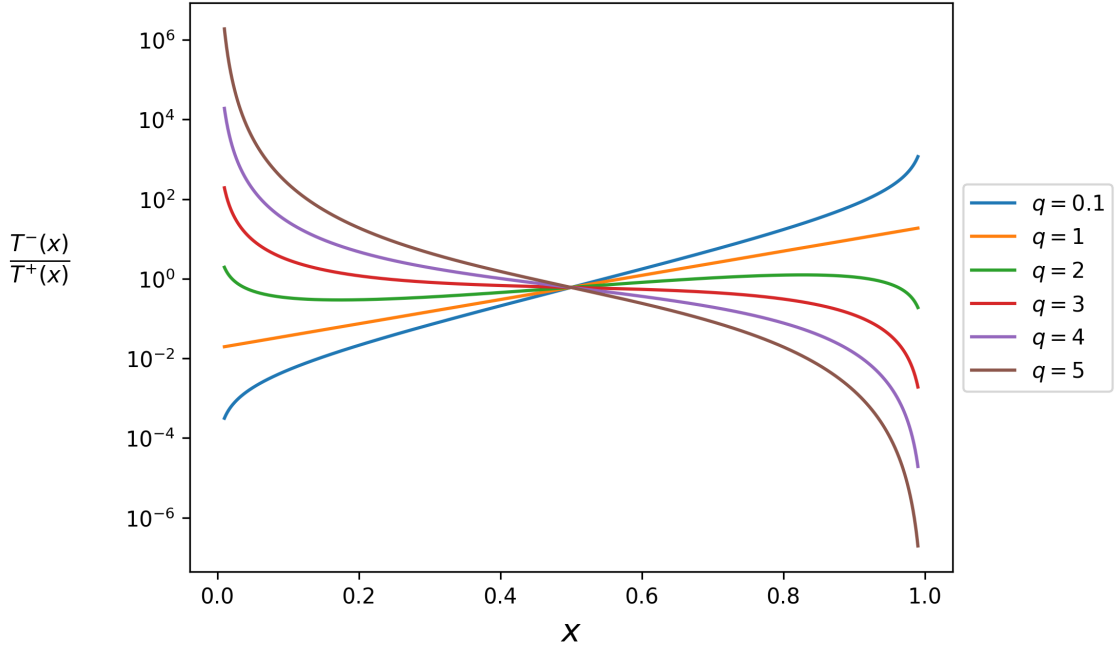


FIG. S2. Ratio $T^-(x)/T^+(x)$ for the system in Figs. 5 and 6. The next event in the population increases the number of mutants (type A) with probability $T^+(x)/[T^+(x) + T^-(x)] = 1/[1 + T^-(x)/T^+(x)]$, or decreases it with probability $1/[1 + T^+(x)/T^-(x)]$.

S4. Pair approximation on graphs

A. Notation

We now analyse q -deformed dynamics on graphs. We assign each node a state $s = \pm 1$ if it is an A or B type respectively. We focus on undirected graphs.

We perform a *homogeneous pair approximation*, similar to [41, 42]. This approximation is known to capture the behaviour of the model to good accuracy on infinite uncorrelated graphs [43]. By uncorrelated graphs we mean graphs where nodes have no preference for attaching to nodes of any particular degree [44].

We write the degree distribution of a general graph as P_k . This is the probability that a randomly chosen node in the graph has degree k (i.e. k neighbours). We denote the number of A type neighbours of a node as n . A node in state s and of degree k with n type A neighbours will often be referred to as an (n, k, s) node.

B. Rate of change of the proportion of agents of type A

We wish to determine a differential equation for $\langle x_+ \rangle$, which we define to be the average density of nodes in the $+1$ state. By average we mean average over independent realisations of the dynamics. The angle-bracket notation is dropped to ease notation and keep consistency with the rest of the paper and the literature. We assume a time step of $dt = \frac{1}{N}$, and take $N \rightarrow \infty$ in order to obtain the continuous-time limit, thus the following now only applies to infinite graphs.

The general rate equation for x_+ is

$$\frac{dx_+}{dt} = \frac{1}{1/N} \sum_{s=\pm 1} T^s \Delta x_+^s, \quad (\text{S26})$$

where T^s is the rate at which $-s$ nodes flip to s nodes, and Δx_+^s is the amount x_+ changes when this happens. The factor $1/N$ in the denominator results from a division by the time-step.

It can be seen by inspection that $\Delta x_+^s = -s/N$, therefore

$$\frac{dx_+}{dt} = T^+ - T^-. \quad (\text{S27})$$

C. The homogeneous pair approximation

Determining the rates T^s will require knowing the probability that a node in state s with degree k has n neighbours in the state $+1$, we will denote this probability $B_s(n|k)$. To derive an expression for $B_s(n|k)$ we will use the *homogeneous pair approximation*. This assumes that the states of the different neighbours are independent, and leads to a binomial distribution of the form

$$B_s(n|k) = \binom{k}{n} p(+1|s)^n [1 - p(+1|s)]^{k-n}, \quad (\text{S28})$$

where $p(+1|s)$ is the single-event probability that a node in state s is connected to a node in state $+1$. This probability can be defined in terms of the density of state- s nodes, x_s , and a quantity σ which is the density of links connecting opposite spin nodes. We refer to σ as the density of active interfaces/links, in-line with standard voter model terminology [41]. The conditional probability $p(+|s)$ can be determined as follows: $p(+|-)$ is the ratio of the number of links connecting opposite-state nodes to the total number of -1 state nodes,

$$p(+|-) = \frac{\sigma \cdot \frac{\mu N}{2}}{x_- \mu N} = \frac{\sigma}{2(1 - x_+)}. \quad (\text{S29})$$

The probability $p(+|+)$ can then be easily determined from

$$\begin{aligned} p(+) &= p(+|-)p(-) + p(+|+)p(+), \\ \implies p(+|+) &= 1 - \frac{\sigma}{2x_+}. \end{aligned} \quad (\text{S30})$$

Thus, combining Eqs. (S29) and (S30) we have the general expression

$$p(+|s) = \frac{1+s}{2} - s \frac{\sigma}{2x_s}. \quad (\text{S31})$$

The moments of $B_s(n|k)$ can then be evaluated. As we will see below, only the first and second moments are needed, which are $\langle n \rangle_s = kp$ and $\langle n^2 \rangle_s = k^2 p^2 + kp(1-p)$ respectively, where p is shorthand for $p(+1|s)$ from Eq. (S31).

We emphasise that we have assumed that the probability of selecting a link connecting nodes in opposite states, σ , is independent of the degree of the nodes which it connects. This is a shortcoming of the homogeneous pair approximation. Extensions have been proposed, such as the heterogeneous pair approximation [34], which allows σ to depend on degree. Similarly, we assume an infinite graph. The stochastic pair approximation [45] accounts for finite-size corrections. However, here, we do not consider these extensions.

D. Rate of change of σ

Due to the presence of σ in the binomial moments, the differential equations for x_+ will be coupled to the differential equation for σ . The general form for such an equation has an analogous form to Eq. (S26),

$$\frac{d\sigma}{dt} = \frac{1}{1/N} \sum_{s=\pm 1} T^s \Delta\sigma^s. \quad (\text{S32})$$

Again T^s is the rate at which $-s$ nodes flip to s nodes. The quantity $\Delta\sigma^s$ is the corresponding change in the density of active links. Assuming it is an $(n, k, -s)$ node that flips to a (n, k, s) node, for $s = +1$ there are n active links initially, and $k - n$ active links after flipping, thus a change of $k - 2n$. There are $\frac{\mu N}{2}$ links overall, so the change in the density of active links is $\frac{2(k-2n)}{\mu N}$. Similar analysis for $s = -1$ gives overall $\Delta\sigma^s = \frac{s(k-2n)}{\mu N}$. Therefore we can write Eq. (S32) as

$$\frac{d\sigma}{dt} = \frac{2}{\mu} [T^+ - T^-] (k - 2n). \quad (\text{S33})$$

E. Transition rates on graphs

The dynamics we have considered so far on complete graphs is a form of pairwise comparison dynamics. A node is chosen at random, q of its neighbours are then chosen. If all q neighbours are of opposite type to the originally selected node, the node will change type with a probability given by the Fermi function [Eq. (6)]. The argument of this function is the payoff difference $\Delta\pi$, i.e. the difference in the average payoff of the node and one of its neighbours. This is fine to do, as on a complete graph all q neighbours have the same payoff (if they are all in the same state).

On general graphs things are different. A node will select q random neighbours, but, even if they are all in the same state, those neighbours do not necessarily have the same average payoff, as they themselves have different neighbourhoods. Instead then on a general graph we replace $\Delta\pi \rightarrow \Delta\pi_{n,k}$ where

$$\begin{aligned} \Delta\pi_{n,k} &\equiv \pi_+(n, k) - \pi_-(n, k) \\ &= a\frac{n}{k} + b\frac{k-n}{k} - c\frac{n}{k} - d\frac{k-n}{k} \\ &= (a-b-c+d)\frac{n}{k} + (b-d) \\ &= u\frac{n}{k} + v. \end{aligned} \quad (\text{S34})$$

Here $\pi_s(n, k)$ is the average payoff of an (n, k, s) node, it is defined analogously to Eq. (2). $\Delta\pi_{n,k}$ then is the increment in the average payoff when an $(n, k, -1)$ node changes to an $(n, k, +1)$ node. In other words, decisions are based on comparing the payoff to one node with the payoff this node would receive if it changed state (and keeping all neighbours in their present state). We thus introduce [Eq. (6)]

$$g_{n,k}^\pm = \frac{1}{1 + e^{\mp\Delta\pi_{n,k}}}. \quad (\text{S35})$$

This gives the probability that an $(n, k, -1)$ node changes to an $(n, k, +1)$ node. When $\Delta\pi_{n,k} \rightarrow \infty$, the average payoff of the node being spin $+1$ is much larger than it being spin -1 , $g_{n,k}^+ \rightarrow 1$ accordingly, meaning the node is guaranteed to flip.

We can now form expressions for T^s which are needed for Eqs. (S27) and (S33). We have

$$T^+ = \sum_{k=1}^{N-1} P_k \sum_{n=0}^k B_-(n|k) x_- \left(\frac{n}{k}\right)^q g_{n,k}^+, \quad (\text{S36a})$$

$$T^- = \sum_{k=1}^{N-1} P_k \sum_{n=0}^k B_+(n|k) x_+ \left(\frac{k-n}{k}\right)^q g_{n,k}^-. \quad (\text{S36b})$$

Consider Eq. (S36a), which is the rate at which the density of +1 nodes increase under our modified pairwise comparison dynamics. For this to happen an $(n, k, -1)$ node must be picked at random, this gives rise to the first three terms. q random neighbours in the state -1 must then be picked, which happens with probability $(\frac{n}{k})^q$. The node must then decide to switch its state with probability $g_{n,k}^+$. Eq. (S36b) has an analogous structure where an $(n, k, +1)$ node becomes an $(n, k, -1)$ node.

We can now substitute Eqs. (S36a) and (S36b) into Eqs. (S27) and (S33) to find

$$\frac{dx_+}{dt} = \sum_k P_k \sum_{n=0}^k \left[x_- \left(\frac{n}{k} \right)^q g_{n,k}^+ B_-(n|k) - x_+ \left(\frac{k-n}{k} \right)^q g_{n,k}^- B_+(n|k) \right], \quad (\text{S37a})$$

$$\frac{d\sigma}{dt} = \frac{2}{\mu} \sum_k P_k \sum_{n=0}^k \left[x_- \left(\frac{n}{k} \right)^q g_{n,k}^+ B_-(n|k) - x_+ \left(\frac{k-n}{k} \right)^q g_{n,k}^- B_+(n|k) \right] (k - 2n). \quad (\text{S37b})$$

F. Analytically tractable limits

We will now evaluate Eqs. (S37a) and (S37b) in some analytically tractable limits to check their validity. These are the voter model (Sec. S4F1) and the complete graph (Sec. S4F2)

1. Voter model limit

The limit $q = 1, \beta = 0$ (since we absorbed β into u and v this means having $u = v = 0$) is the standard voter model and Eqs. (S37a) and (S37b) should reproduce known results from [41].

Eq. (S37a) becomes

$$\begin{aligned} \frac{dx_+}{dt} &= \frac{1}{2} \sum_k P_k \sum_{n=0}^k \left\{ x_- \left(\frac{n}{k} \right) B_-(n|k) - x_+ \left(1 - \frac{n}{k} \right) B_+(n|k) \right\} \\ &= \frac{1}{2} \sum_k P_k \left\{ x_- \left(\frac{\langle n \rangle_-}{k} \right) - x_+ \left(1 - \frac{\langle n \rangle_+}{k} \right) \right\} \\ &= \frac{1}{2} \sum_k P_k \left\{ x_- \left(\frac{\sigma}{2x_-} \right) - x_+ \left(\frac{\sigma}{2x_+} \right) \right\} \\ &= 0, \end{aligned} \quad (\text{S38})$$

where $\langle n \rangle_s$ is the first moment of the binomial distribution $B_s(n|k)$ defined in Eq. (S28). So the average density of nodes in state +1 does not change with time as expected in the standard voter model.

Eq. (S37b) becomes

$$\begin{aligned} \frac{d\sigma}{dt} &= \frac{1}{\mu} \sum_k P_k \sum_{n=0}^k \left\{ x_- \left(\frac{n}{k} \right) B_-(n|k) - x_+ \left(1 - \frac{n}{k} \right) B_+(n|k) \right\} (k - 2n) \\ &= \frac{1}{\mu} \sum_k P_k \left\{ x_- \left(\langle n \rangle_- - 2 \frac{\langle n^2 \rangle_-}{k} \right) - x_+ \left(k - 3 \langle n \rangle_+ + 2 \frac{\langle n^2 \rangle_+}{k} \right) \right\} \\ &= \frac{1}{\mu} \sum_k P_k \left\{ (k-2)\sigma - \frac{(k-1)\sigma^2}{2x_+(1-x_+)} \right\} \\ &= \frac{1}{\mu} \left\{ (\mu-2)\sigma - \frac{(\mu-1)\sigma^2}{2x_+(1-x_+)} \right\}, \end{aligned} \quad (\text{S39})$$

where $\langle n^2 \rangle_s$ is the second moment of the binomial distribution $B_s(n|k)$ defined in Eq. (S28). With the replacement $x_+ \rightarrow x$, and moving to the steady-state we find

$$\sigma_{\text{st}} = 2 \left(\frac{\mu - 2}{\mu - 1} \right) x_{\text{st}} (1 - x_{\text{st}}), \quad (\text{S40})$$

where x_{st} is the long-term stationary fraction of agents of type A . The pre-factor describes the long-lived plateau of the density of active links reported in [41].

2. Complete graph limit

The degree distribution of a complete graph is a delta function peaked around N , i.e. $P_k \rightarrow \delta(k - N)$. Furthermore, the binomial distributions defined in Eq. (S28) are also delta functions peaked around Nx_+ , i.e. $B_s(n|k) \rightarrow \delta(n - Nx_+)$. This is because every node is connected and there are Nx_+ nodes in state +1, so the probability any node has Nx_+ neighbours is 1, and 0 for any other number of +1 neighbours.

With this, and using the notation $x_+ \rightarrow x$, Eq. (S37a) becomes

$$\dot{x} = (1 - x)x^q g^+(x) - x(1 - x)^q g^-(x), \quad (\text{S41})$$

where the standard Fermi function, Eq. (6), has reappeared due to the delta functions acting on $g_{n,k}^\pm$ [Eq. (S35)]. Thus we recover Eq. (8), which applies for well-mixed populations.

Similarly, Eq. (S37b) becomes

$$\begin{aligned} \frac{d\sigma}{dt} &= 2(1 - 2x) \left[(1 - x)x^q g^+(x) - x(1 - x)^q g^-(x) \right] \\ &= 2(1 - 2x)\dot{x}, \end{aligned} \quad (\text{S42})$$

where we have used Eq. (S41). This is exactly as expected. As on an infinite complete graph with a fraction x nodes in state +1, there are $N^2x(1 - x)$ active links and $\frac{N^2}{2}$ links overall, thus $\sigma = 2(x - x^2)$. So we expected $\frac{d}{dt}\sigma = 2(1 - 2x)\dot{x}$, which is exactly what we see in Eq. (S42).

G. Degree-regular graphs

For degree-regular graphs Eqs. (S37a) and (S37b) simplify significantly. The degree distribution is simply a delta function peaked at $\mu \in \mathbb{Z}_{\geq 2}$, i.e. $P_k \rightarrow \delta(k - \mu)$, which collapses the outer summations over k , so we have

$$\frac{dx_+}{dt} = \sum_{n=0}^{\mu} \left[x_- \left(\frac{n}{\mu} \right)^q g_{n,\mu}^+ B_-(n|\mu) - x_+ \left(\frac{\mu - n}{\mu} \right)^q g_{n,\mu}^- B_+(n|\mu) \right], \quad (\text{S43a})$$

$$\frac{d\sigma}{dt} = \frac{2}{\mu} \sum_{n=0}^{\mu} \left[x_- \left(\frac{n}{\mu} \right)^q g_{n,\mu}^+ B_-(n|\mu) - x_+ \left(\frac{\mu - n}{\mu} \right)^q g_{n,\mu}^- B_+(n|\mu) \right] (\mu - 2n). \quad (\text{S43b})$$

This pair of coupled differential equations can be numerically integrated and in Fig. S3 we show some example trajectories for a single degree-regular graph, varying the parameter q . The approximation works fairly well given the coarse nature of the pair approximation.

To classify the dynamics for a given set of parameters we can look at multiple pair approximation trajectories for different initial densities of ± 1 type nodes, this is shown in Fig. S4. For $q = 0.5$ there is a stable fixed point at around $x_+ = 0.7$, thus the flow could be classified as co-existence type. This is in-line with the idea that small values of q promote the minority, as discussed for complete graphs in Sec. S2. For $q = 1$ (standard game dynamics) there is a stable fixed point at $x_+ = 1$, which is unsurprising as the parameters chosen correspond to an A -dominance type flow for complete graphs [see Sec. S2]. For $q = 2$ there appears to be an unstable fixed point just below $x_+ = 0.4$, thus this flow could be classified as co-ordination type. Again this is in line with Sec. S2 where we found large values of q promote the majority.

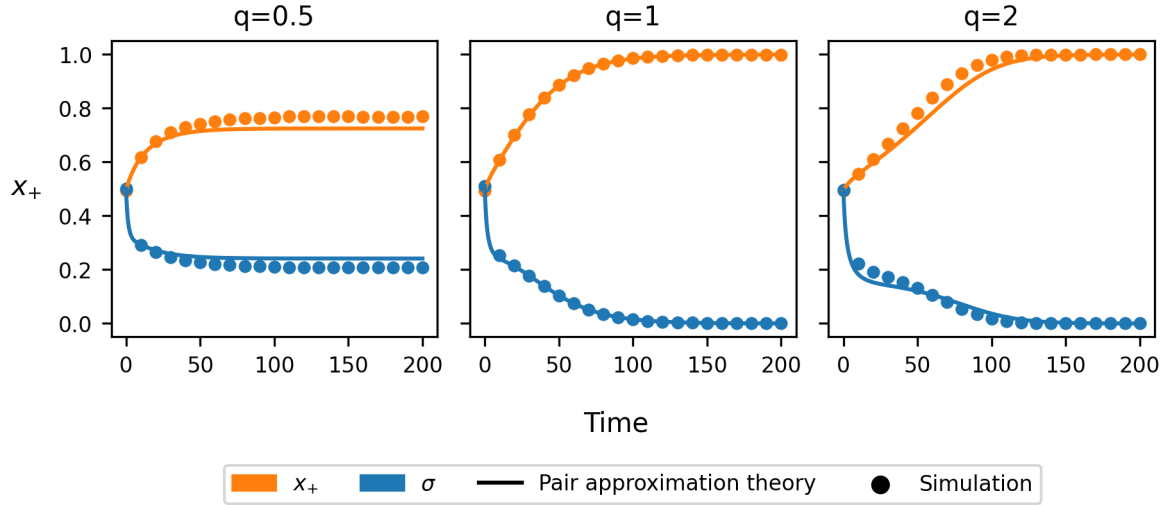


FIG. S3. Plot showing the time evolution of the density of nodes in state $+1$ x_+ (orange), and density of active links σ (blue) for different values of q , starting from a random state where $x_+ = 0.5$. The game parameters are $u = 0.1$ and $v = 0.1$. The underlying topology is a degree-regular graph with $N = 10,000$ and $\mu = 3$. Solid lines are analytical solutions from numerically integrating Eqs. (S43a) and (S43b). Circle markers are from averaging 100 independent Gillespie simulations of the dynamics.

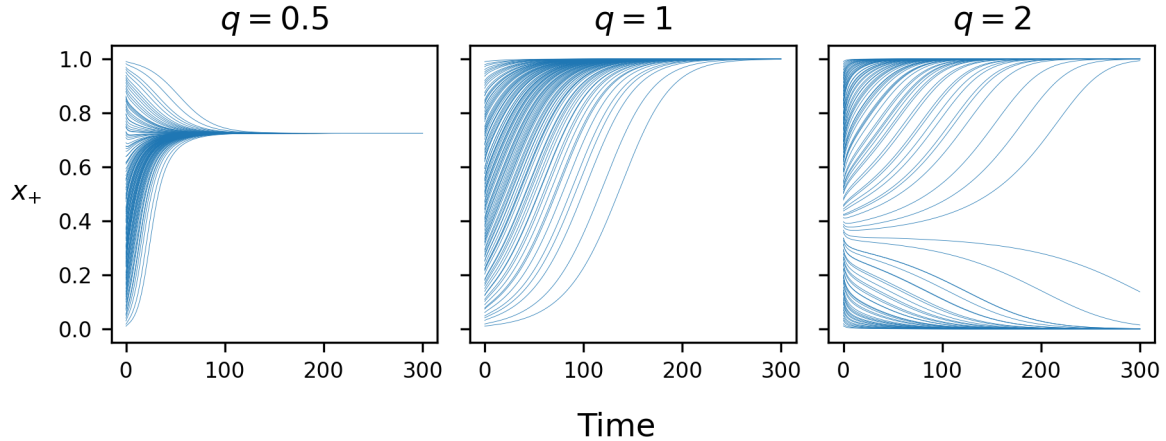


FIG. S4. Pair approximation trajectories from numerically integrating Eqs. (S43a) and (S43b) for different values of q and initial densities of ± 1 type nodes. The model parameters are $u = 0.1$ and $v = 0.1$. The theoretical underlying degree-regular graph has $\mu = 3$ and is of infinite size.

H. Non-regular graphs

The case of graphs which are not regular is more difficult. We use Eqs. (S37a) and (S37b) but we have to perform the summation over the degree distribution P_k .

We show in Figs. S5 and S6 analogous plots to Figs. S3 and S4 but now for Barabási–Albert and Erdős–Rényi graphs respectively to demonstrate the validity of the solution for different heterogeneous uncorrelated (or approximately uncorrelated) graphs.

We note that in Fig. S5 the analytical results agree very well with simulation, even more than for degree-regular graphs (Fig. S3). This is likely because in Fig. S3 $\mu = 3$ whereas in Fig. S5 $\mu = 8$. This form of pair approximation is known to breakdown at lower μ [34].

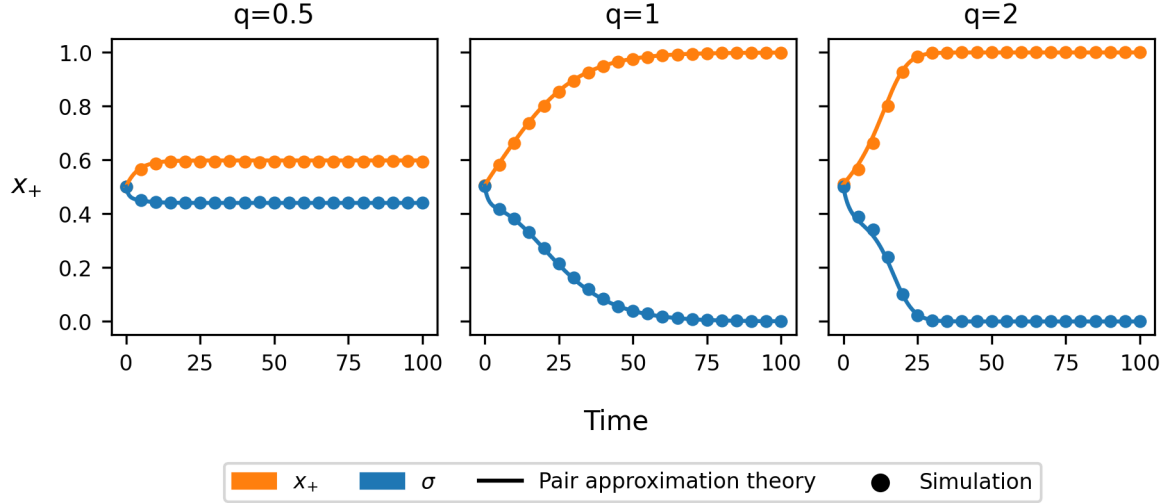


FIG. S5. Plot showing the time evolution of the density of nodes in state +1 x_+ (orange), and density of active links σ (blue) for different values of q , starting from a random state where $x_+ = 0.5$. The game parameters are $u = 0.1$ and $v = 0.1$. The underlying topology is a Barabási-Albert graph with $N = 10,000$ where each node connects to 4 existing nodes so that $\mu = 8$. Solid lines are analytical solutions from numerically integrating Eqs. (S37a) and (S37b). Circle markers are from averaging 100 independent Gillespie simulations of the dynamics.

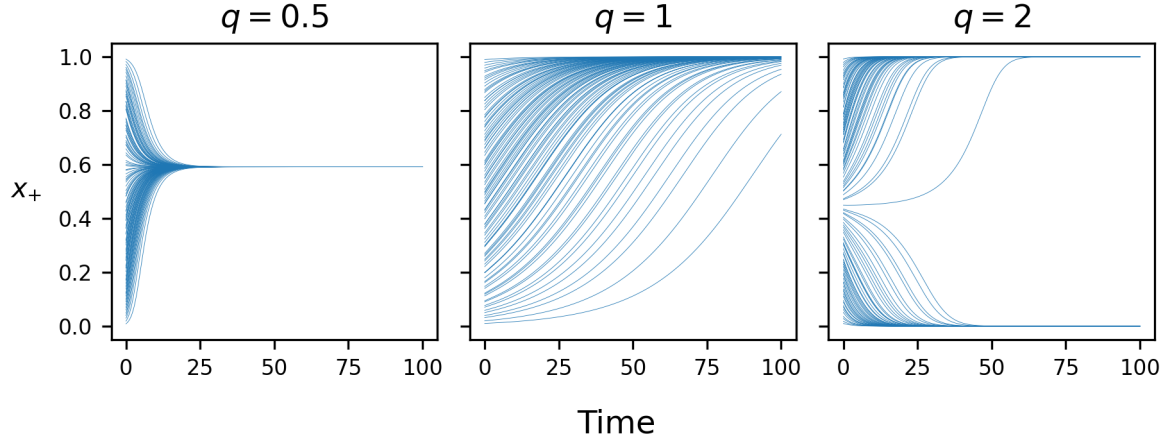


FIG. S6. Pair approximation trajectories from numerically integrating Eqs. (S37a) and (S37b) for different values of q and initial densities of ± 1 type nodes. The model parameters are $u = 0.1$ and $v = 0.1$. The underlying Erdős-Rényi graph has $N = 10,000$ and $p = 8/N$ so that $\mu \approx 8$.

S5. q -deformed dynamics for cyclic games

We wish to determine the classification of the q -deformed dynamics for cyclic games [such as the rock-paper-scissors (RPS) game]. In this appendix we study games defined by the payoff matrix

$$\begin{array}{ccc} & \text{R} & \text{P} & \text{S} \\ \text{R} & \begin{pmatrix} 0 & a & b \\ b & 0 & a \\ a & b & 0 \end{pmatrix} \end{array} \quad (\text{S44})$$

This is a generalisation of Eq. (26). We study the dynamics for general $q \in \mathbb{R}^+$ and $a, b \in \mathbb{R}$.

The centre of the strategy simplex $(\frac{1}{3}, \frac{1}{3}, \frac{1}{3})$ is always a fixed point, as are the pure strategies at the corners of the simplex. We thus study the linear stability of these fixed points. We note that there are only two degrees of freedom in the system since $\sum_i x_i = 1$.

An accompanying Mathematica notebook with further details of the following calculations can be found at a GitHub repository [46].

A. The centre point

Here we analyse the stability of the point $p_{\text{centre}} = (\frac{1}{3}, \frac{1}{3}, \frac{1}{3})$. The Jacobian of the dynamics in Eq. (25) (after reduction to two degrees of freedom) evaluated at the centre is

$$\mathbf{J}_{\text{centre}} = \begin{pmatrix} \frac{1}{2 \cdot 3^q} (3q - 3 - b) & \frac{1}{2 \cdot 3^q} (a - b) \\ -\frac{1}{2 \cdot 3^q} (a - b) & \frac{1}{2 \cdot 3^q} (3q - 3 - a) \end{pmatrix}. \quad (\text{S45})$$

The eigenvalues of this matrix are,

$$\lambda^{\pm} = \frac{1}{4 \cdot 3^q} \left[6q - 6 - (a + b) \pm i|a - b|\sqrt{3} \right]. \quad (\text{S46})$$

Assuming $a \neq b$, both eigenvalues are complex, and thus the point p_{centre} can only be a centre, spiral sink, or spiral source [47]. For centres, we require the real part of the eigenvalues to be zero, this occurs when

$$q = q_c \equiv 1 + \frac{a + b}{6}. \quad (\text{S47})$$

When $q < q_c$, the real part of both eigenvalues is negative, so p_{centre} will be a spiral sink. When $q > q_c$, the real part of both eigenvalues is positive, so p_{centre} will be a spiral source.

In the special case of $a = b$, we have a single real eigenvalue with algebraic multiplicity 2,

$$\lambda = \frac{1}{2 \cdot 3^q} (3q - 3 - a). \quad (\text{S48})$$

The eigenspace has geometric multiplicity 2, i.e. there are two linearly independent eigenvectors corresponding to this eigenvalue, namely $(\begin{smallmatrix} 1 \\ 0 \end{smallmatrix})$ and $(\begin{smallmatrix} 0 \\ 1 \end{smallmatrix})$. This means that p_{centre} is a star, which is a source when $\lambda > 0$, i.e. $q > 1 + \frac{a}{3}$, and a sink when $\lambda < 0$, i.e. $q < 1 + \frac{a}{3}$. When $q = 1 + \frac{a}{3}$ we have a centre once again.

For general a and b then, p_{centre} is some form of sink when $q < q_c$, some form of source when $q > q_c$, and a centre when $q = q_c$.

B. The corners

Here we analyse the stability of the corners, p_{corner} , i.e. permutations of the point $(1, 0, 0)$. By symmetry all corners give the same results from stability analysis.

1. $q = 1$

When $q = 1$ the eigenvalues of $\mathbf{J}_{\text{corner}}$ are

$$\lambda_1 = \tanh\left(\frac{a}{2}\right), \quad (\text{S49a})$$

$$\lambda_2 = \tanh\left(\frac{b}{2}\right). \quad (\text{S49b})$$

Thus both eigenvalues are real. If both $a, b > 0$, then the corners are **sources**. If both $a, b < 0$, then the corners are **sinks**. If a and b have opposite signs then the corners are **saddle points**.

For $a = b = 0$ all entries in the payoff matrix are zero. There is thus no actual game dynamics, and the flow is solely determined by the q -deformation. For the case $q = 1$ (no deformation), which we are discussing here, this means that there is no dynamics at all ($\dot{x}_i = 0$ for all i).

2. $q > 1$

When $q > 1$ the eigenvalues of $\mathbf{J}_{\text{corner}}$ are

$$\lambda_1 = \frac{-1}{1 + e^a}, \quad (\text{S50a})$$

$$\lambda_2 = \frac{-1}{1 + e^b}. \quad (\text{S50b})$$

Thus for all a, b both eigenvalues are real and negative, hence the corners are always **sinks**.

3. $0 < q < 1$

For any q the rate equations are (after reduction to two degrees of freedom, which we will call x and y , these are the proportions of two of the strategies):

$$\begin{aligned} \frac{dx}{dt} = x^q & \left[\frac{1-x-y}{1+\exp\{a(x-y)-b(1-x-2y)\}} + \frac{y}{1+\exp\{a(1-x-2y)-b(1-2x-y)\}} \right] \\ & - x \left[\frac{(1-x-y)^q}{1+\exp\{-a(x-y)+b(1-x-2y)\}} + \frac{y^q}{1+\exp\{-a(1-x-2y)+b(1-2x-y)\}} \right], \end{aligned} \quad (\text{S51a})$$

$$\begin{aligned} \frac{dy}{dt} = y^q & \left[\frac{1-x-y}{1+\exp\{-a(1-2x-y)-b(x-y)\}} + \frac{x}{1+\exp\{-a(1-x-2y)+b(1-2x-y)\}} \right] \\ & - y \left[\frac{(1-x-y)^q}{1+\exp\{a(1-2x-y)+b(x-y)\}} + \frac{x^q}{1+\exp\{a(1-x-2y)-b(1-2x-y)\}} \right]. \end{aligned} \quad (\text{S51b})$$

The right-hand sides evaluate to zero at the corners of the strategy simplex ($x = y = 0$, $x = 1, y = 0$, and $x = 0, y = 1$ respectively). Due to the symmetry with respect to interchange of types, it is sufficient to study the stability of the fixed point at one of the three corners, here we choose $x = y = 0$. For x and y small, but non-zero, and keeping in mind that we focus on $0 < q < 1$, the leading order terms on the right are proportional to x^q or y^q . Therefore, linear stability analysis cannot be used. When both x and y are small, Eqs. (S51a) and (S51b) reduce to

$$\frac{dx}{dt} = \frac{x^q}{1 + e^{-b}}, \quad (\text{S52a})$$

$$\frac{dy}{dt} = \frac{y^q}{1 + e^{-a}}. \quad (\text{S52b})$$

Therefore, both $\dot{x}, \dot{y} > 0$ for x, y small (but positive). This is the case for all a and b , so the corners are always **sources**.

C. Reduction to one-parameter family of payoff matrices

We have shown in Sec. S5B that the stability of the corners is independent of a and b , except when $q = 1$ where only the signs of a and b matter. In Sec. S5A we showed that $a + b$ determines the stability of the centre.

In principle our analysis allows for a complete classification of the flows (as far as linear stability analysis goes) for all values of a, b and q .

In order to reduce the number of parameters we now fix $a = -1$ and focus on positive values of b . This reflects the scenario of a cyclic game. Each strategy is beaten by one other strategy, and in turns beats the remaining strategy. It is convenient to set $b = 1 + \delta$ (following [36]). In this way $\delta = 0$ reflects the standard zero-sum rock-paper-scissors game. The constraint $b > 0$ translates into $\delta > -1$. We note that other (equivalent) setups have been used, see for example [37]. For this reduced setup Eq. (S47) becomes

$$q_c(\delta) = 1 + \frac{\delta}{6}. \quad (\text{S53})$$

The centre fixed point is a stable spiral for $q < q_c(\delta)$ and an unstable spiral for $q > q_c(\delta)$. It is a centre for $q = q_c(\delta)$.

The corners are sources for $q < 1$ and sinks for $q > 1$, as this is independent of δ . For $q = 1$ the corners are saddle points for all $\delta > -1$, otherwise they are sinks.

D. Further ternary plots

As mentioned in Sec. S5 A, when $a = b$ (or in the reduced setup $\delta = -2$) the centre point is a stable or unstable star depending on the value of q .

For $q < q_c(-2)$ the centre point is a stable star. As shown in Sec. S5 B the corners in this region are sources. This leads to trajectories moving directly towards the centre point as illustrated in Fig. S7(a)

For $q_c(-2) \leq q < 1$ the centre point is now an unstable star. Again the corners in this region are sources. This leads to stable fixed points that are inside the simplex as illustrated by the green markers in Fig. S7(b). We note that stable internal fixed points could arise anywhere in the green region in Fig. 8, not just for $\delta = -2$. However, when δ moves further from -2 the centre becomes a stronger spiral sink/source, which forces trajectories into stable orbits rather than to stable fixed points.

For $q \geq 1$ the centre point is still an unstable star but the corners becomes sinks. This leads to trajectories moving directly away from the centre point, converging at the corners as illustrated in Fig. S7(c).

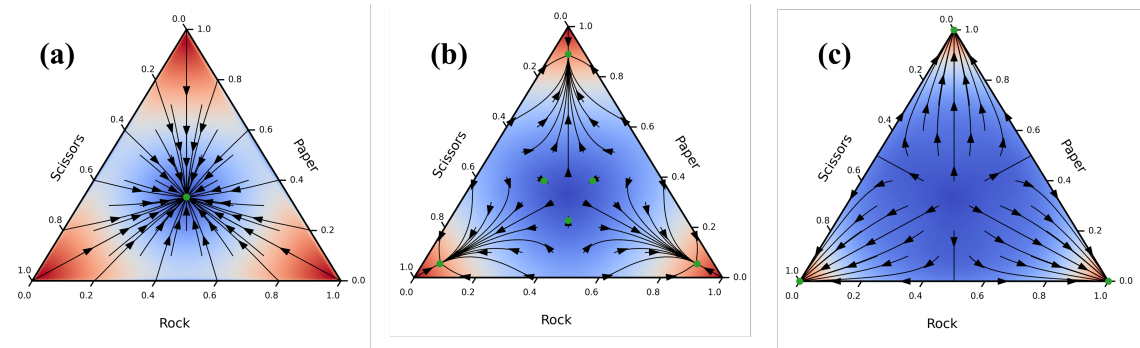


FIG. S7. Ternary plots for the 3-strategy q -deformed evolutionary dynamics under the payoff matrix given in Eq. (26) for $\delta = -2$ and $q = [0.2, 0.7, 1.5]$ in (a), (b) and (c) respectively. Green markers show stable fixed points.

S6. Fixation probability for q -deformed dynamics without replacement for 2×2 games

As in Sec. S3 A we want to calculate the fixation probability ϕ_i , except now for an adapted version of the model where we select an integer number q of neighbours without replacement.

The rates for the model without replacement are defined as follows:

$$T_i^+ = \begin{cases} 0, & 0 \leq i < q \\ (N-i)g_i^+ \prod_{k=1}^q \left(\frac{i-k+1}{N-k} \right), & q \leq i \leq N \end{cases} \quad (\text{S54a})$$

$$T_i^- = \begin{cases} ig_i^- \prod_{k=1}^q \left(\frac{N-i-k+1}{N-k} \right), & 0 \leq i \leq N-q \\ 0, & N-q < i \leq N \end{cases} \quad (\text{S54b})$$

Fig. S8 illustrates the rates for the cases of $q \leq \frac{N}{2}$ and $q > \frac{N}{2}$. We see that it is often the case that the system is driven to one of the absorbing states at $i = 0$ or $i = N$. For $q \leq \frac{N}{2}$ and $q \leq i \leq N-q$ both T_i^+ and T_i^- are non-zero so the system can move in either direction. For $q > \frac{N}{2}$ and $N-q < i < q$ both T_i^+ and T_i^- are 0 so the system does not move. This is because we require at least q A or B agents in order for a node to choose q neighbours of the opposite type.

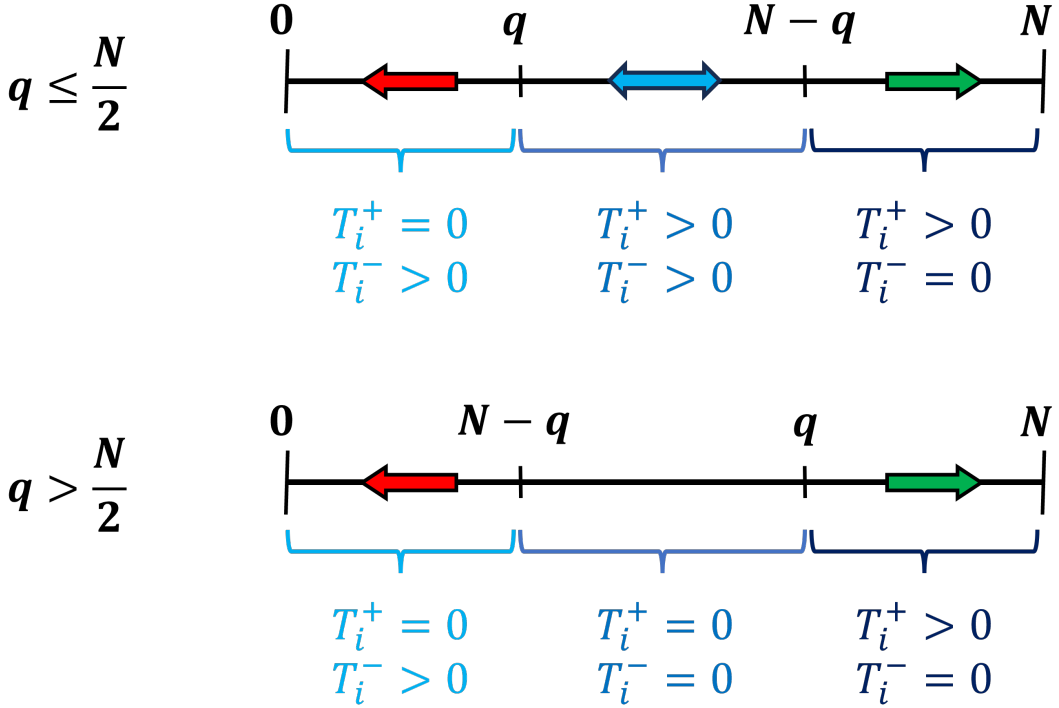


FIG. S8. Demonstration of how the transition rates from Eqs. (S54a) and (S54b) change based on the number of type A agents, i . Top panel shows the case $q \leq \frac{N}{2}$. For $i < q$ or $i > N-q$ the system is always driven to $i = 0$ or $i = N$ respectively. For $q \leq i \leq N-q$ both T_i^+ and T_i^- are finite so the system can move in either direction. The bottom panel shows the case for $q > \frac{N}{2}$. If $i \leq N-q$ or $i \geq q$ the system is always driven to $i = 0$ or $i = N$ respectively. For $q < i < N-q$ both T_i^+ and T_i^- are 0 so the system does not move.

For the case $q \leq \frac{N}{2}$, the probability to fixate with all agents being A type is trivially 0 if $i < q$ and 1 if $i > N-q$. For $q \leq i \leq N-q$ we write the recursive expression

$$\phi_i = T_i^- \phi_{i-1} + T_i^+ \phi_{i+1} + (1 - T_i^- - T_i^+) \phi_i. \quad (\text{S55})$$

Rearranging this equation, and defining $y_i = \phi_i - \phi_{i-1}$, we find $y_{i+1} = \gamma_i y_i$, where $\gamma_i = T_i^- / T_i^+$ is the ratio of the transmission rates. Unlike in the model with replacement [Eq. (S18)], γ_i has a piecewise definition:

$$\gamma_i = \begin{cases} \infty, & 0 \leq i < q, \\ \frac{i}{N-1} \frac{g_i^-(i)}{g_i^+(i)} \prod_{k=1}^q \left(\frac{N-i-k+1}{i-k+1} \right), & q \leq i \leq N-q \\ 0, & N-q < i \leq N \end{cases} \quad (\text{S56})$$

Noting that ϕ_q is the smallest non-zero ϕ , we can write

$$\begin{aligned} y_q &= \phi_q - \phi_{q-1} = \phi_q, \\ y_{q+1} &= \gamma_q y_q = \gamma_q \phi_q, \\ &\vdots \\ y_k &= \phi_q \prod_{j=q}^{k-1} \gamma_j, \end{aligned} \tag{S57}$$

for $k \geq q$. Now, assuming $i \geq q$ we can manipulate ϕ_i into the following form,

$$\begin{aligned} \phi_i &= (\phi_q - \phi_{q-1}) + (\phi_{q+1} - \phi_q) + \dots + (\phi_i - \phi_{i-1}) \\ &= y_q + y_{q+1} + \dots + y_i \\ &= \sum_{k=q}^i y_k \\ &= \phi_q \sum_{k=q}^i \prod_{j=q}^{k-1} \gamma_j, \end{aligned} \tag{S58}$$

noting the first line is possible as all values other than ϕ_{q-1} , which is zero anyway, cancel. In going from the third to fourth line we use Eq. (S57). To determine ϕ_q we use the largest ϕ_i that we know to be equal to one, i.e. ϕ_{N-q+1} ,

$$\begin{aligned} \phi_{N-q+1} &= 1 = \sum_{k=q}^{N-q+1} y_k = \phi_q \sum_{k=q}^{N-q+1} \prod_{j=q}^{k-1} \gamma_j, \\ \implies \phi_q &= \frac{1}{\sum_{k=q}^{N-q+1} \prod_{j=q}^{k-1} \gamma_j}. \end{aligned} \tag{S59}$$

Substituting Eq. (S59) into Eq. (S58) we get an expression for the fixation probability in the intermediate regime,

$$\phi_i = \frac{\sum_{k=q}^i \prod_{j=q}^{k-1} \gamma_j}{\sum_{k=q}^{N-q+1} \prod_{j=q}^{k-1} \gamma_j}. \tag{S60}$$

When $q > \frac{N}{2}$ all cases are trivial. $i \leq N - q$ and $i \geq q$ give ϕ_i as 0 or 1 respectively as the system is forced to the absorbing states. The intermediate case of $N - q < i < q$ gives $\phi_i = 0$, as the system cannot move. Overall then for $q > \frac{N}{2}$ we have $\phi_i = 0$ for $0 \leq i < q$, and $\phi_i = 1$ for $q \leq i \leq N$.

Combining all results we have for the fixation probability:

$$\phi_i = \begin{cases} 0, & (q \leq \frac{N}{2} \text{ and } 0 \leq i < q) \text{ or } (q > \frac{N}{2} \text{ and } 0 \leq i < q) \\ \frac{\sum_{k=q}^i \prod_{j=q}^{k-1} \gamma_j}{\sum_{k=q}^{N-q+1} \prod_{j=q}^{k-1} \gamma_j}, & q \leq \frac{N}{2} \text{ and } q \leq i \leq N - q \\ 1, & (q \leq \frac{N}{2} \text{ and } N - q < i \leq N) \text{ or } (q > \frac{N}{2} \text{ and } q \leq i \leq N) \end{cases} \tag{S61}$$

[1] John von Neumann. Zur theorie der gesellschaftsspiele. *Mathematische annalen*, 100(1):295–320, 1928.
[2] John Von Neumann. On the theory of games of strategy. *Contributions to the Theory of Games*, 4:13–42, 1959.
[3] John Von Neumann and Oskar Morgenstern. Theory of games and economic behavior. In *Theory of games and economic behavior*. Princeton university press, 2007.
[4] John Maynard Smith and George R Price. The logic of animal conflict. *Nature*, 246(5427):15–18, 1973.
[5] John Maynard Smith. *Evolution and the Theory of Games*. Cambridge university press, 1982.
[6] Herbert Gintis. *Game theory evolving*. Princeton University Press, Princeton, 2000.

- [7] Josef Hofbauer and Karl Sigmund. Evolutionary game dynamics. *Bulletin of the American mathematical society*, 40(4):479–519, 2003.
- [8] Christine Taylor, Drew Fudenberg, Akira Sasaki, and Martin A. Nowak. Evolutionary game dynamics in finite populations. *Bulletin of Mathematical Biology*, 66(6):1621–1644, 2004.
- [9] Arne Traulsen, Jens Christian Claussen, and Christoph Hauert. Coevolutionary dynamics: from finite to infinite populations. *Physical review letters*, 95(23):238701, 2005.
- [10] Arne Traulsen and Christoph Hauert. Stochastic evolutionary game dynamics. *Reviews of nonlinear dynamics and complexity*, 2:25–61, 2009.
- [11] Erez Lieberman, Christoph Hauert, and Martin A. Nowak. Evolutionary dynamics on graphs. *Nature*, 433:312–316, 2005.
- [12] Arne Traulsen, Jens Christian Claussen, and Christoph Hauert. Coevolutionary dynamics in large, but finite populations. *Phys. Rev. E*, 74:011901, 2006.
- [13] Jens Christian Claussen. Drift reversal in asymmetric coevolutionary conflicts: influence of microscopic processes and population size. *Eur. Phys. J. B*, 60:391–399, 2007.
- [14] Alex J Bladon, Tobias Galla, and Alan J McKane. Evolutionary dynamics, intrinsic noise, and cycles of cooperation. *Phys. Rev. E*, 81(6):066122, 2010.
- [15] Arne Traulsen, Martin A Nowak, and Jorge M Pacheco. Stochastic dynamics of invasion and fixation. *Physical Review E*, 74(1):011909, 2006.
- [16] Richard A Holley and Thomas M Liggett. Ergodic theorems for weakly interacting infinite systems and the voter model. *The annals of probability*, pages 643–663, 1975.
- [17] Boris L Granovsky and Neal Madras. The noisy voter model. *Stochastic Processes and their applications*, 55(1): 23–43, 1995.
- [18] Mauro Mobilia, Anna Petersen, and Sidney Redner. On the role of zealotry in the voter model. *Journal of Statistical Mechanics: Theory and Experiment*, 2007(08):P08029, 2007.
- [19] Naoki Masuda. Voter models with contrarian agents. *Physical Review E—Statistical, Nonlinear, and Soft Matter Physics*, 88(5):052803, 2013.
- [20] Claudio Castellano, Santo Fortunato, and Vittorio Loreto. Statistical physics of social dynamics. *Reviews of modern physics*, 81(2):591–646, 2009.
- [21] Sidney Redner. Reality-inspired voter models: A mini-review. *Comptes Rendus Physique*, 20(4):275–292, 2019.
- [22] Claudio Castellano, Miguel A Muñoz, and Romualdo Pastor-Satorras. Nonlinear q-voter model. *Physical Review E*, 80(4):041129, 2009.
- [23] Mauro Mobilia. Nonlinear q -voter model with inflexible zealots. *Phys. Rev. E*, 92:012803, 2015.
- [24] Lucía S. Ramirez, Federico Vazquez, Maxi San Miguel, and Tobias Galla. Ordering dynamics of nonlinear voter models. *Phys. Rev. E*, 109:034307, 2024.
- [25] Lawrence E Blume. The statistical mechanics of strategic interaction. *Games and economic behavior*, 5(3):387–424, 1993.
- [26] André M Timpanaro and Carmen PC Prado. Exit probability of the one-dimensional q -voter model: Analytical results and simulations for large networks. *Physical Review E*, 89(5):052808, 2014.
- [27] Andrew Mellor, Mauro Mobilia, and RKP Zia. Characterization of the nonequilibrium steady state of a heterogeneous nonlinear q -voter model with zealotry. *Europhysics Letters*, 113(4):48001, 2016.
- [28] Arkadiusz Jedrzejewski. Pair approximation for the q -voter model with independence on complex networks. *Physical Review E*, 95(1):012307, 2017.
- [29] Piotr Nyczka, Katarzyna Sznajd-Weron, and Jerzy Cisło. Phase transitions in the q -voter model with two types of stochastic driving. *Physical Review E—Statistical, Nonlinear, and Soft Matter Physics*, 86(1):011105, 2012.
- [30] Philipp M Altrock and Arne Traulsen. Fixation times in evolutionary games under weak selection. *New Journal of Physics*, 11(1):013012, 2009.
- [31] The supplement contains further details of the model and the theoretical and numerical analysis (url to be inserted by copy editor), 2024.
- [32] Martin A Nowak. *Evolutionary dynamics: exploring the equations of life*. Harvard university press, 2006.
- [33] Milton Abramowitz and Irene A Stegun. *Handbook of mathematical functions with formulas, graphs, and mathematical tables*, volume 55. US Government printing office, 1948.
- [34] Emanuele Pugliese and Claudio Castellano. Heterogeneous pair approximation for voter models on networks. *Europhysics Letters*, 88(5):58004, 2009.
- [35] György Szabó and Gábor Fáth. Evolutionary games on graphs. *Physics Reports*, 446(4):97–216, 2007.
- [36] Qian Yu, Debin Fang, Xiaoling Zhang, Chen Jin, and Qiyu Ren. Stochastic evolution dynamic of the rock–scissors–paper game based on a quasi birth and death process. *Scientific reports*, 6(1):28585, 2016.
- [37] Mauro Mobilia. Oscillatory dynamics in rock–paper–scissors games with mutations. *Journal of Theoretical Biology*, 264(1):1–10, 2010. ISSN 0022-5193.
- [38] Philipp M. Altrock, Chaitanya S. Gokhale, and Arne Traulsen. Stochastic slowdown in evolutionary processes. *Phys. Rev. E*, 82:011925, 2010.
- [39] Philipp M. Altrock, Arne Traulsen, and Tobias Galla. The mechanics of stochastic slowdown in evolutionary games. *Journal of Theoretical Biology*, 311:94–106, 2012.
- [40] Laura Hindersin and Arne Traulsen. Most undirected random graphs are amplifiers of selection for birth-death dynamics, but suppressors of selection for death-birth dynamics. *PLOS Computational Biology*, 11(11):1–14, 11

2015.

- [41] Federico Vazquez and Víctor M Eguíluz. Analytical solution of the voter model on uncorrelated networks. *New Journal of Physics*, 10(6):063011, 2008.
- [42] Christopher R Kitching, Henri Kauhanen, Jordan Abbott, Deepthi Gopal, Ricardo Bermúdez-Otero, and Tobias Galla. Estimating transmission noise on networks from stationary local order. *arXiv preprint arXiv:2405.12023*, 2024.
- [43] James P Gleeson. Binary-state dynamics on complex networks: Pair approximation and beyond. *Physical Review X*, 3(2):021004, 2013.
- [44] Sergey Dorogovtsev. *Lectures on Complex Networks*. Oxford University Press, 02 2010.
- [45] Antonio F Peralta, Adrián Carro, M San Miguel, and Raúl Toral. Stochastic pair approximation treatment of the noisy voter model. *New Journal of Physics*, 20(10):103045, 2018.
- [46] Christopher R. Kitching. q-deformed evolutionary dynamics in simple matrix games, May 2024. URL <https://github.com/C-Kitching/q-deformed-evolutionary-dynamics-in-simple-matrix-games>.
- [47] Steven H Strogatz. *Nonlinear dynamics and chaos with student solutions manual: With applications to physics, biology, chemistry, and engineering*. CRC press, 2018.